Materials Today Bio 32 (2025) 101751

Contents lists available at ScienceDirect

Materials Today Bio

journal homepage: www.journals.elsevier.com/materials-today-bio

An NIR-responsive "4A hydrogel" encapsulating wormwood essential oil: through antibacterial, antioxidant, anti-inflammation, and angiogenic to promote diabetic wound healing

Mengjuan Tao [a,b,1], Zhiwei Sun [a,1], Haiyan Wang [c,1], Na Meng [d,1], Xiangru Chen [a], Jianwei Mao [e], Heyan Huang [a], Yan Huang [a], Jin Liu [f], Zhenxing Wang [g], Weiqiang Tan [h], Yonggang Chen [b,*], Chuchao Zhou [a,**], Yanqing Yang [a,***]

[a] Department of Plastic Surgery, Tongren Hospital of Wuhan University (Wuhan Third Hospital), Wuhan, Hubei, 430060, PR China
[b] Department of Clinical Laboratory, Wuhan Center for Clinical Laboratory, Wuhan, Hubei, 430015, PR China
[c] Chinese Medical Association Wuhan Branch, Wuhan, Hubei, 430014, PR China
[d] Department of Cardiology, Guiqian International General Hospital, Guiyang, Guizhou, 550018, PR China
[e] Department of Hepatobiliary Surgery, Xiaogan Center Hospital, Xiaogan, Hubei, 430071, PR China
[f] Hubei Engineering & Technology Research Center for Functional Materials from Biomass, School of Chemistry and Material Science, Hubei Engineering University, Xiaogan, Hubei, 432000, PR China
[g] Department of Plastic Surgery, Union Hospital, Tongji Medical College, Huazhong University of Science and Technology, Wuhan, Hubei, 430022, PR China
[h] Department of Plastic Surgery, Sir Run Run Shaw Hospital, Zhejiang University School of Medicine, 3 East Qingchun road, Hangzhou, 310016, PR China

ARTICLE INFO

Keywords:
Wormwood essential oil
Black phosphorus
Multifunctional hydrogel
Microenvironment

ABSTRACT

The incorporation of hydrogels with biocompatible functional components to develop wound dressings exhibiting potent antibacterial, antioxidant, anti-inflammatory, and angiogenic properties to promote diabetic wound healing is highly desirable yet continues to pose a significant challenge. In this study, wormwood essential oil (WEO) is successfully encapsulated within black phosphorus (BP) using a physical extrusion technique. Subsequently, this composite is encapsulated within biocompatible gelatin methacrylate (GelMA) and hyaluronic acid methacrylate (HAMA) hydrogels to create multifunctional hydrogel dressing (WEO@BP/GH). In comparison to traditional hydrogels, BP enhances the encapsulation stability of WEO and improves the microenvironmental regulation capabilities through NIR-triggered release of WEO. Systemic in vitro experiments demonstrate that synergistic interaction between the diverse bioactive components of WEO and photothermal effects of BP results in highly effective antibacterial activities against *S. aureus* and *E. coli*, antioxidant of scavenging ROS, anti-inflammation of downregulating M1/M2 macrophages ratio, and angiogenic properties. Moreover, the in vivo tests demonstrate that WEO@BP/GH hydrogel significantly enhances high-performance diabetic wound repair through the acceleration of hemostasis, promotion of collagen deposition, regulation of inflammatory responses, and facilitation of vascularization. The findings indicate that WEO@BP/GH hydrogel holds considerable promise as a candidate for microenvironment regulation and effective diabetic wound healing across various clinical applications.

1. Introduction

Diabetes mellitus is a significant public health issue due to its link to rising mortality and morbidity rates [1,2]. By 2045, around 700 million people are expected to have diabetes, with many at risk of developing diabetic wounds (DW) [3,4]. These wounds often become chronic and non-healing because of factors like metabolic stress, hypoxia, ischemia, and infection [5,6]. A DW often becomes stuck in a harmful

* Corresponding author.
** Corresponding author.
*** Corresponding author.
E-mail addresses: chenyonggang@wuhanccl.com (Y. Chen), TR000050@whu.edu.cn (C. Zhou), TR000047@whu.edu.cn (Y. Yang).
[1] These authors have contributed equally to this work.

https://doi.org/10.1016/j.mtbio.2025.101751
Received 5 January 2025; Received in revised form 23 March 2025; Accepted 9 April 2025
Available online 9 April 2025

inflammatory cycle due to factors like impaired growth factor response, poor circulation, ongoing proinflammatory cytokine release, excess reactive oxygen species (ROS), and other microvascular issues [7,8]. Basic wound care may be insufficient, necessitating targeted interventions at different healing stages due to the multifactorial nature of DW complications [9,10]. Despite the rapid growth of diabetic patients worldwide, there are currently no effective therapeutic strategies for diabetic wound healing, which underscores the need to identify new therapeutic approaches.

Recently, interest has surged in using hydrogels for biomaterials-based microenvironment modulation [11–13]. Hydrogels, made of hydrophilic polymers, can retain water at wound sites and offer stability through their cross-linked network, making them ideal for localized wound management [14,15]. They stand out in tissue repair and regeneration by enabling the incorporation of bioactive molecules or cells [16,17]. Bioactive molecules in hydrogels can be gradually released for sustained therapeutic effects [18,19]. Among various strategies, ROS-scavenging hydrogels are commonly used [8,20]. Many nanoparticles are loaded in hydrogels for ROS-scavenging, including self-propelled nanovesicles and PtCuTe nanosheets [21–23]. However, solely targeting ROS is ineffective in addressing hyperinflammation, persistent infection, and ischemia in diabetic wound healing [24,25]. Thus, we aimed to create a wound dressing with enhanced microenvironment regulation and wound-healing properties.

Advancements in phytochemistry have led to the use of essential oils as mild microenvironment regulation agents due to their bioactive components [26]. The main components of wormwood essential oil include camphor, eugenol, and germacrene D. They have rich biological effects, including antibacterial, anti-inflammatory, ROS-scavenging, and promoting the polarization of M2-type macrophages. These rich effects can effectively regulate the microenvironment of diabetic wounds, thus promoting the healing of diabetic wounds [1]. However, their hydrophobic nature complicates integration with hydrophilic hydrogel dressings, and their volatility limits effective penetration into biofilms, reducing their effectiveness in treating diabetic wounds [27,28]. Encapsulating essential oils in colloidal delivery systems with surfactants improves their payload and water stability [29]. However, many surfactants, particularly anionic and cationic types, can disrupt lipid membranes and cause skin irritation, limiting their biocompatibility [30]. Additionally, surfactant-stabilized emulsions often lack thermal stability, complicating their use in thermal polymerization [4,31]. Therefore, efficiently integrating hydrophobic essential oils with hydrophilic hydrogels to create a biocompatible wound dressing that enhances microenvironment regulation is crucial for improving diabetic wound healing.

Photothermal therapy (PTT) is a novel approach that utilizes photothermal agents (PTAs) to convert the optical energy of near-infrared (NIR) light into localized physical heat energy. PTT has several advantages of broad-spectrum antibacterial activity, deep tissue penetration, and good biosafety, which making PTT gradually become an ideal treatment strategy to replace antibiotic therapy [32,33]. Black phosphorus (BP) generally shows strong absorption of NIR radiation and excellent photothermal conversion due to its adjustable bandgap (0.3–2.0 eV) [34]. This can greatly improve the effectiveness and safety of photothermal treatment in biomedical applications, particularly for minimally invasive, effective sterilization in anti-infection diabetic wound treatments [35,36]. BP can degrade and form phosphate in the environment of oxygen and water, making the surface of black phosphorus negatively charged and hydrophilic. Hydrophilic BP, combined with its unique planar structure and large specific surface area, can form oil-in-water particles with hydrophobic essential oils, thus effectively loading the essential oil [37,38]. Additionally, the degraded non-toxic phosphate and phosphonate by BP in biological environments can integrate safely into human phosphorus metabolism [39,40]. Therefore, the development of BP nanoplatforms loaded with essential oils, which have a combination of NIR response, the ability to regulate the microenvironment, and improved wound healing, is an intriguing strategy for diabetic wounds.

In this study, BP nanosheets and photo-crosslinking 3D network were used to integrate natural wormwood essential oil (WEO) with biocompatible gelatin methacrylate (GelMA) and hyaluronic acid methacrylate (HAMA) hydrogel to construct a class of "4A Hydrogel" wound dressing with antibacterial, antioxidant, anti-inflammation, and angiogenic activities (Fig. 1). A nanoparticle extruder was employed to create a nano shelter structure with BP nanosheets on the exterior and WEO inside. Gelatin methacrylate (GelMA) and hyaluronic acid methacrylate (HAMA) were photo-crosslinked to form a stable 3D network capable of drug loading. This structure effectively encapsulated WEO in the BP nanosheets and hydrogel, creating a microenvironment-regulating hydrogel dressing (WEO@BP/GH). Unlike traditional hydrogel-based WEO delivery, BP nanosheets boost loading efficiency, provide NIR-responsive release, and enhance the antibacterial properties of WEO@BP/GH through a synergistic photothermal effect. In addition, the 3D network of WEO@BP/GH provides excellent swelling and hemostatic properties, allowing for effective exudate absorption and bleeding prevention. Its abundant hydroxyl and amino groups enhance skin adhesion, making it suitable for clinical use. These features enable WEO@BP/GH hydrogel to effectively heal diabetic wounds in rats, highlighting its potential for treating acute wounds and chronic infectious wounds.

2. Results and discussion

2.1. Fabrication and physicochemical characterization

Wound dressings play a crucial role in wound management by acting as a protective barrier against external infections and serving as a scaffold to facilitate the reorganization of skin cells, as well as the infiltration and integration of host tissues, thereby significantly enhancing the wound healing process [41]. An optimal skin wound dressing should fulfill several key criteria: (1) excellent biocompatibility, ensuring it does not induce toxicity or inflammation; (2) effective moisture retention, which maintains a moist wound environment conducive to cell hydration and possesses the capacity to absorb wound exudate. (3) adequate physical and mechanical strength to maintain structural integrity and prevent the infiltration of external bacteria due to material failure; and (4) an optimal surface microstructure and biochemical properties to facilitate cell adhesion, proliferation, and differentiation [42,43]. Consequently, selecting suitable materials and proper structure is vital to construct wound dressings with good biocompatibility, superior physicochemical properties, and rich biological characteristics.

2.1.1. Preparation and characterization of WEO@BP nanoparticles

BP nanosheets were meticulously selected as carriers for the fabrication of WEO-in-BP nanoparticles via a physical extrusion technique utilizing 400 nm polycarbonate membranes. The BP nanosheets were synthesized through a modified liquid exfoliation process of BP bulk [34]. The lamellar structure of the dispersed nanosheets was characterized using scanning electron microscopy (SEM) and transmission electron microscopy (TEM), as depicted in Figs. S1A and C. Additionally, energy-dispersive X-ray spectrometry (EDX) analysis confirmed the presence of phosphorus within the nanosheets, as shown in Fig. S1B. The majority of the BP nanosheets (80.33 %) exhibited a diameter distribution within the range of 0–396 nm (Fig. S1D), consistent with the dimensions of BP nanosheets documented in existing literature [39]. The atomic force microscopy (AFM) image confirms the two-dimensional sheet-like morphology of the BP nanosheets, with an average thickness measured at 5.58 ± 1.72 nm (Figs. S1E and F). These findings suggest the successful fabrication of BP nanosheets.

The schematic representation of the structure and controlled release mechanism of WEO@BP nanoparticles is depicted in Fig. 2A. SEM and

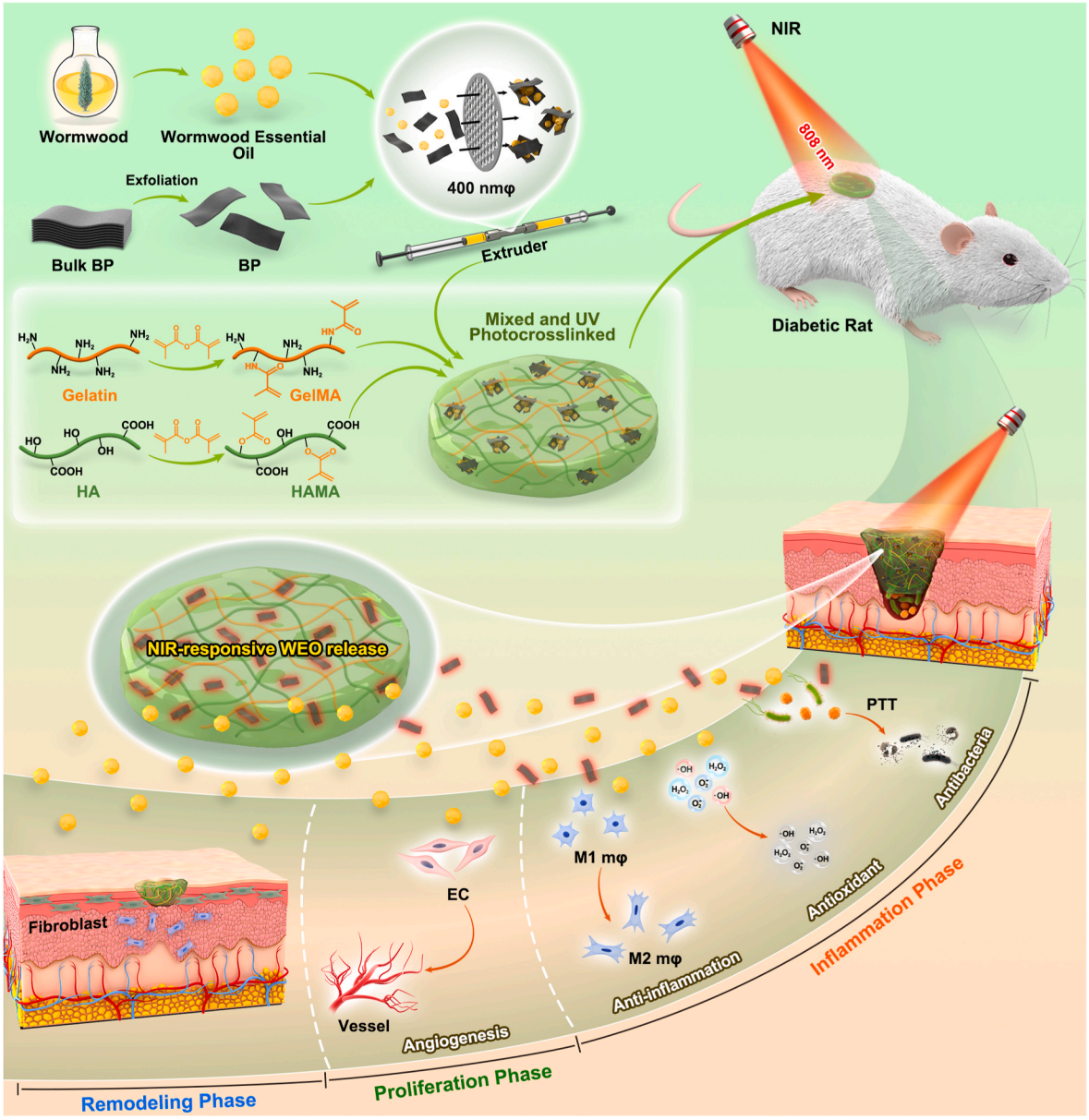

Fig. 1. Schematic illustration of the preparation of the WEO@BP/GH hydrogel and its mechanism to promote diabetic wound healing through antibacterial, antiinflammation, antioxidant, and angiogenic properties.

TEM analyses revealed spherical structures of WEO, as shown in Fig. 2B and D. Following extrusion through an extruder, the WEO nanoparticles were encapsulated within BP nanosheets, as illustrated in Fig. 2C and E. The size distribution of the WEO@BP nanoparticles was determined using dynamic light scattering (DLS), with the majority (88.88 %) of the particles measuring between 0 and 400 nm (Fig. 2F). Specifically, the peak values at 200 nm and 400 nm correspond to the particles of WEO and WEO@BP, respectively. The size of these particles is consistent with the results observed under SEM and TEM. The encapsulation efficiency (EE%) and loading capacity (LC%) of WEO within the WEO nanohydrogels were calculated to be 58.2 % and 3.6 %, respectively. This demonstrates the substantial WEO-loading capacity attained by the nanocarriers. The chemical composition of the synthesized WEO was analyzed using gas chromatography (GC), as depicted in Fig. 2G. The analysis identified eucalyptol, camphor bicyclo[5.2.0]nooane, furan, 2-ethyl-5-methyl-, bicyclo[2.2.1]heptan-2-ol, trans-Chrysanthenol, thujoneBicyclo[3.1.0] hexan-3-one, and terpinyl formate (Table S1), which collectively constituted 31.9 % of the total content. To assess the controlled release of WEO@BP/GH hydrogels, near-infrared (NIR) laser irradiation was utilized. Following a 5-min period of NIR irradiation, a significant increase in the release of WEO was observed. Furthermore, following three cycles of irradiation, the cumulative release of WEO reached 32.73 %. Hydrogels subjected to NIR irradiation exhibited a significantly higher release rate compared to those not exposed to NIR irradiation (Fig. 2H). Extending the observation period to 120 h resulted in the release of a majority of the WEO (91.94 %), which was substantially higher than that observed in hydrogels without NIR irradiation (Fig. 2I). These findings demonstrate the successful construction of WEO@BP nanoparticles with an effective NIR-responsive release capability.

2.1.2. *Fabrication and characterization of the hydrogels*

Optical images of the fabricated hydrogels were collected (Fig. 3A). Transparent white color was observed in GH hydrogel, while black color was observed in BP/GH hydrogel. The uniform black color of BP/GH hydrogel indicated that BP nanosheets were dispersed evenly in GH

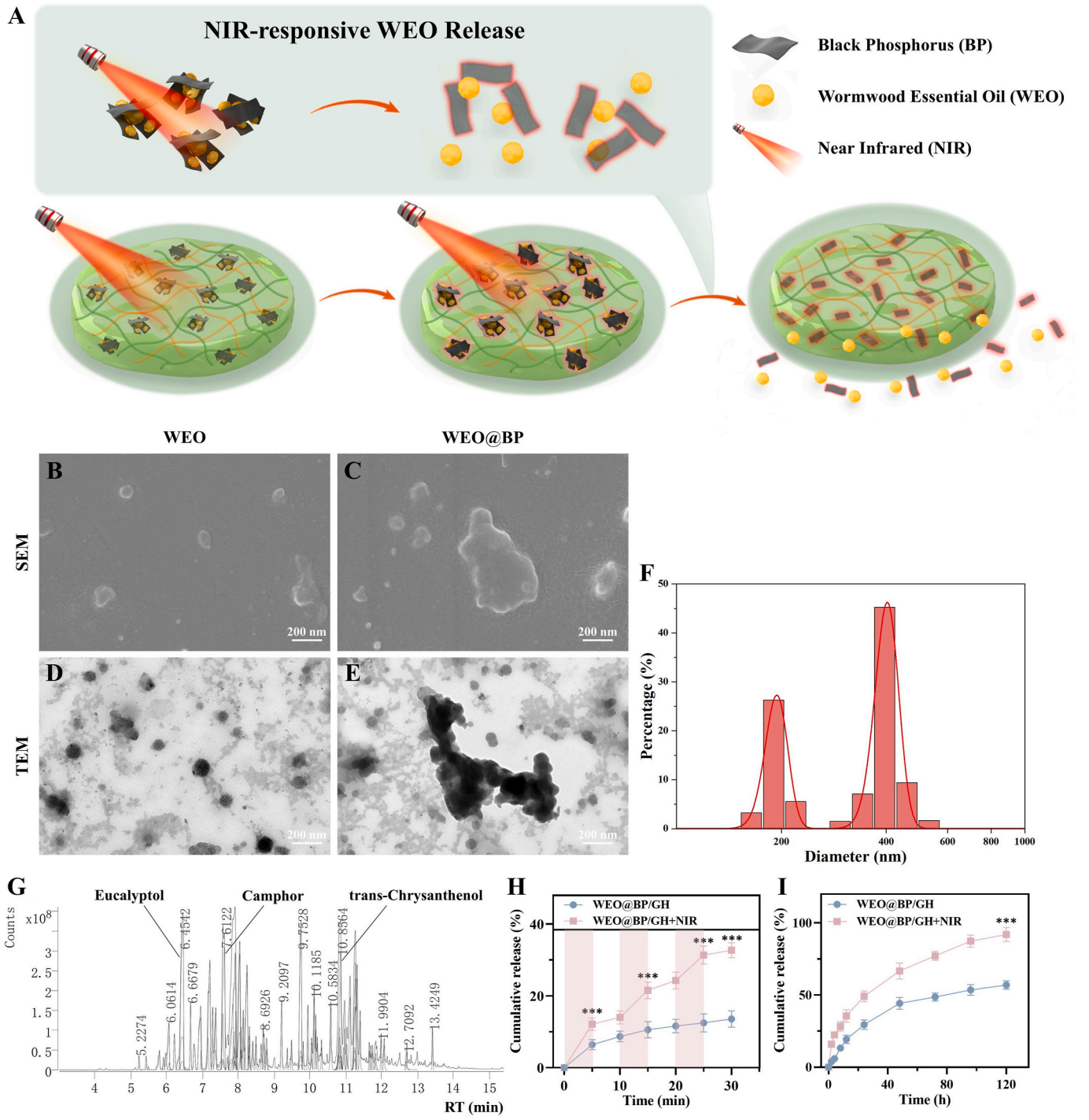

Fig. 2. Fabrication and characterization of the WEO@BP nanoparticles. A) Schematic illustration of the fabrication and NIR-trigged release of the WEO@BP nanoparticles. B, C) SEM images of WEO and WEO@BP nanoparticles, respectively. Scale bar: 200 nm. D, E) TEM images of WEO and WEO@BP nanoparticles, respectively. Scale bar: 200 nm. F) DLS evaluation of WEO@BP nanoparticles. G) Gas chromatography analysis of WEO nanoparticles. H, I) Cumulative release of WEO@BP/GH hydrogels with and without NIR irradiation within 30 min (H) and 120 h (I).

hydrogel. After introducing WEO into the BP/GH hydrogel, the color of hydrogel changed into gray. This may be owing to the dilution of the BP nanosheets resulting in the fading of color, and the combination of WEO and BP resulting in the blocking of the color of BP was also an important reason. To conduct a more detailed examination of the microscopic topology of hydrogels, SEM was employed on freeze-dried hydrogel samples (Fig. 3B). The GH, BP/GH, and WEO@BP/GH hydrogels demonstrated a porous, three-dimensional interconnected architecture, which is conducive to exudate absorption and cellular proliferation [44, 45]. Particularly, SEM images at higher magnifications revealed that the interior surface of the GH hydrogel appeared smooth, while the interior of the WEO@BP/GH hydrogel exhibited a rough texture. This roughness is attributed to the incorporation of WEO@BP nanoparticles, as indicated by the red arrows. In order to evaluate the effect of different GelMA/HAMA ratios on the structure of hydrogels, four kinds of hydrogels (5G2H, 15G2H, 10G5H, and 10G10H) were prepared and observed under SEM (Fig. S2A). It can be seen that the pore size of all groups of hydrogels was small and uneven, which was not conducive to

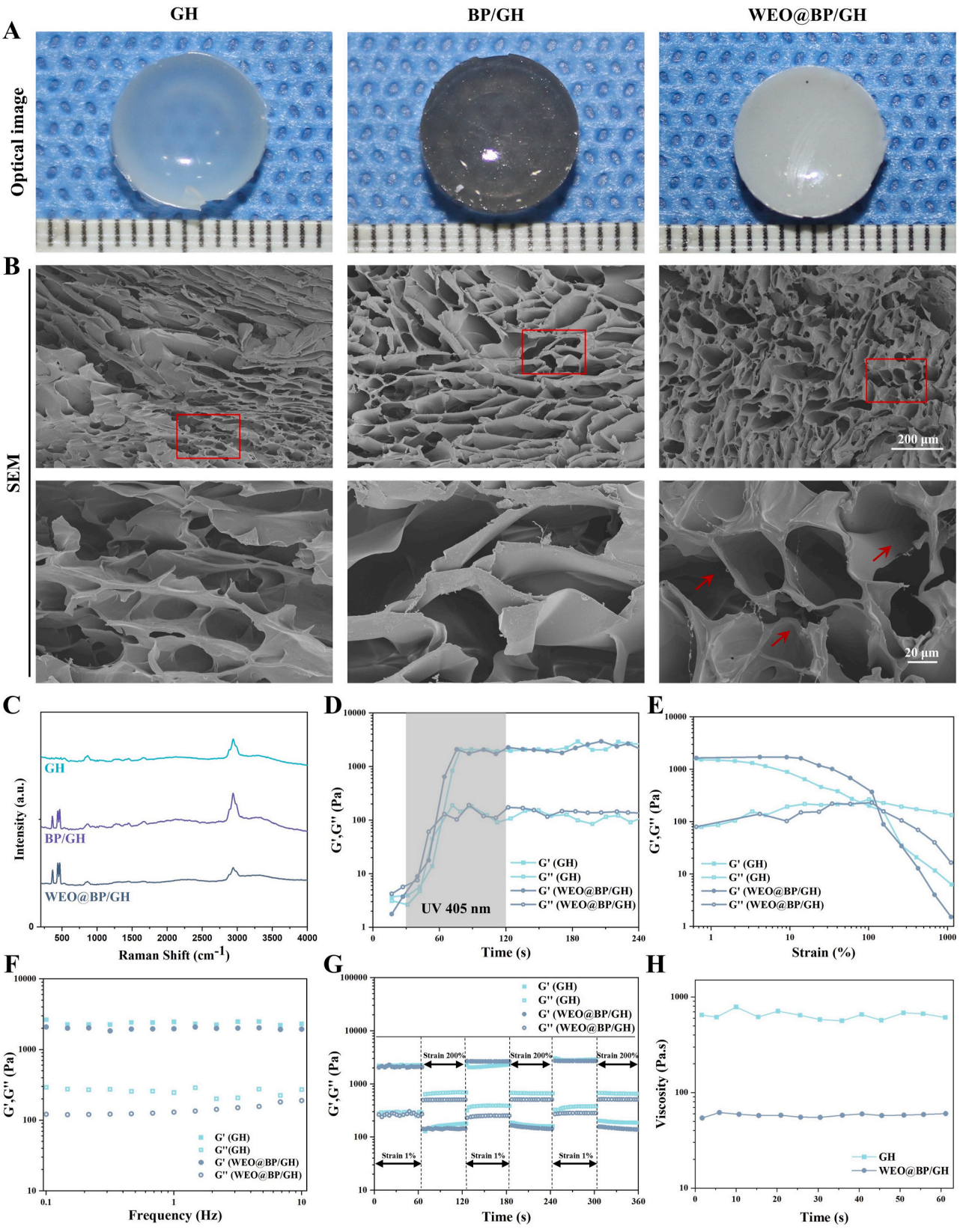

Fig. 3. Physiochemical characterization of the hydrogels. A) Optical images of the fabricated GH, BP/GH, and WEO@BP/GH hydrogels. B) SEM images of the hydrogels at different magnifications. The red arrow refers to WEO@BP nanoparticles. Scale bar in low magnification: 200 μm. Scale bar in high magnification: 20 μm. C) Raman spectra of the hydrogels. D) Dynamic rheological evaluation of the UV-crosslinking processes of GH and WEO@BP/GH hydrogels. E-H) Rheological analysis of the strain sweep (E), dynamic step-strain (F), frequency sweep (G), and viscosity (H) of GH and WEO@BP/GH hydrogels. (For interpretation of the references to color in this figure legend, the reader is referred to the Web version of this article.)

the exchange of nutrients and the expansion of cells [46,47].

To verify the chemical structure of the scaffolds, Fourier Transform Infrared (FTIR) spectroscopy was conducted, as depicted in Fig. S3A. The observed stretching vibrations of the dissociated carboxyl group (-COO^-) at 1420 cm^{-1} and the methylene group (-CH_2) at 2923 cm^{-1} confirm the successful modification of carboxymethyl groups in GH. Additionally, the asymmetrical deformation vibration associated with the protonation of the amine group (-NH_3^+) at 1595 cm^{-1}, along with the stretching vibrations of aromatic amines (-CN) at 1321 cm^{-1}, indicate the presence of amino groups in GH [48]. The stretching vibrations of amide I (1645 cm^{-1}) and the bending vibrations of amide II (1591 cm^{-1}) suggest the formation of amide bonds (-NHCO-) within the hydrogels as a result of UV-induced crosslinking reactions [49,50]. However, the FTIR spectroscopy was unable to detect the presence of BP nanosheets within the BP/GH and WEO@BP/GH hydrogels, likely due to the low concentration of BP (0.3 % w/v) incorporated. Raman spectroscopy, on the other hand, is extensively utilized for the characterization of carbon-based materials, primarily because the presence of conjugated and double carbo-carbon bonds results in significant Raman signal intensities [34,51]. In this study, the Raman spectrum was employed to identify the components of the hydrogels, as illustrated in Fig. 3C. The characteristic peaks corresponding to BP were observed at 354, 433, and 462 cm^{-1} within the BP/GH and WEO@BP/GH hydrogels, indicating the successful incorporation of BP into the GH hydrogel matrix [52]. These findings, corroborated by both FTIR and Raman spectroscopy, confirm the successful synthesis of the WEO@BP/GH hydrogel.

Subsequently, we assessed the water uptake and retention properties of the hydrogels. The water uptake profiles (Fig. S4A) indicated similar absorption patterns among the GH, BP/GH, and WEO@BP/GH hydrogels. An initial rapid water uptake was observed within the first 5 min, transitioning to a gradual stabilization after 240 min. Under equilibrium conditions, the water absorption rate of GH (11.4 ± 0.4 %) exceeded that of WEO@BP/GH (9.4 ± 0.3 %), implying that the incorporation of WEO@BP enhanced the crosslinking characteristics of the hydrogel [3]. To evaluate the water retention capacity, the hydrogels were subjected to a drying process within a fume hood maintained at 37 °C until their weights stabilized, indicating no further changes. The WEO@BP/GH hydrogels demonstrated a slightly enhanced water retention capacity compared to GH, as illustrated in Fig. S4B. These results suggest that the WEO@BP/GH hydrogels synthesized in this study possess exceptional water uptake and retention properties. Consequently, they are well-suited for effectively absorbing wound exudates and maintaining an optimal moisture environment, which is essential for the healing of DW [52,53].

Successively, the rheological characteristics of GH and WEO@BP/GH hydrogels were comprehensively assessed. Hydrogel dressings were required to exhibit adequate mechanical resilience and self-healing properties to adapt effectively to the dynamic and intricate microenvironment of wounds [14,54]. As illustrated in Fig. 3D, exposure to ultraviolet irradiation resulted in a substantial enhancement of the hydrogel's mechanical properties, with the storage modulus (G′) increasing approximately 100-fold from 10 Pa to 1000 Pa. Furthermore, strain sweep experiments were performed to determine the linear viscoelastic region of the hydrogels (Fig. 3E). The WEO@BP/GH hydrogel exhibited a gelation threshold at approximately 100 % strain, signifying a transition to a colloidal state beyond this strain level. Furthermore, we investigated the frequency-dependent rheological properties by employing oscillatory frequencies ranging from 0.1 to 10 Hz (Fig. 3F). Across the tested frequency spectrum, the storage modulus (G′) of all hydrogels consistently exceeded the loss modulus (G″), thereby confirming their elastic nature [55,56]. In addition, dynamic amplitude tests were performed to evaluate the self-healing properties of hydrogels. Fig. 3G demonstrated the application of a substantial strain amplitude of 200 % to disrupt the cross-linked hydrogel network, followed by a mild strain amplitude of 1 % to assess the hydrogel's recovery capacity. At a strain amplitude of 200 %, the G′ exhibited a less pronounced reduction compared to the G″, indicating the occurrence of fracturing within the hydrogel. However, upon reducing the strain back to 1 %, both G′ and G″ returned to their original values, signifying a rapid recovery of the hydrogel. The cyclic disruption and reformation of the hydrogel network demonstrated its exceptional self-healing capabilities. Furthermore, the viscosity of the WEO@BP/GH hydrogel exhibited consistent stability over time (shear rate: 10 rad/s, 37 °C), indicating strong adhesion of the synthesized hydrogel (Fig. 3H) [57,58]. Based on these findings, the WEO@BP/GH hydrogels exhibited enhanced mechanical properties and self-healing abilities, facilitating their seamless application and intended function in complex diabetic wound environments.

2.2. Microenvironment regulation performances in vitro

Wound healing is a complex process with four stages: hemostasis, inflammation, proliferation, and remodeling, involving various cells and cytokines [59,60]. Unlike acute wounds, diabetic wounds heal slower due to ongoing inflammation, high oxidative stress, stubborn infections, and reduced growth factor activity [7,8]. In addition, chronic hyperglycemia hinders new vessel formation, restricting oxygen and nutrient supply to wounds [6,61]. While diabetic wounds heal similarly to normal wounds, they often stagnate at some stage, especially in the inflammation stage, due to a disrupted microenvironment [62]. Regulating this microenvironment is crucial for the orderly progression of the four stages of diabetic wound healing.

2.2.1. Hemostasis and hemolysis assessment

The hemostasis stage initiates wound healing, and an ideal wound dressing should quickly stop bleeding with minimal or no hemolysis [53,63]. Rat tail injury models tested the hydrogel's hemostatic effectiveness under bleeding conditions (Figs. S5A and B) [44]. Normal PBS resulted in 111.4 ± 14.0 mg bleeding on filter papers, whereas hydrogels and gauze showed minimal blood loss (<50.0 mg). In addition, the hydrogel's hemocompatibility was also evaluated by an in vitro hemolysis assay [64]. GH, BP/GH, WEO@BP/GH, and WEO@BP/GH + NIR hydrogels were incubated with blood at 37 °C for 24 h, then centrifuged to obtain supernatants. Fig. S6A showed that these supernatants were nearly colorless with red blood cells settled at the bottom, similar to the negative 0.9 % NaCl control. In contrast, the positive 0.1 % Triton X-100 group was vividly red. The hemolysis rates for the hydrogel groups were below 5 %, indicating they were safe for medical use (Fig. S6B) [65]. These findings confirmed that our hydrogels did not cause hemolysis. In general, the tests indicated that incorporating WEO@BP into the GelMA-HAMA hydrogel was non-toxic, showing effective hemostasis and low hemolysis. This may be due to: (1) The hydrogel's stable crosslinking network, which minimizes nanoparticle's explosive release into red blood cells, and (2) BP nanosheets degrading into non-toxic substances in biological environments [36,66].

2.2.2. Photothermal performances of the hydrogels in vitro

The NIR photothermal properties of WEO@BP/GH hydrogels were thoroughly studied. Hydrogels were exposed to an 808 nm laser at different power levels, and infrared images were taken (Fig. 4A). After 5 min of exposure, WEO@BP/GH hydrogel reached temperatures of 38.8 °C, 55.6 °C, and 69.4 °C at 0.5 W cm^{-2}, 1.0 W cm^{-2}, and 1.5 W cm^{-2}, respectively (Fig. 4B). Additionally, the WEO@BP/GH hydrogels maintained consistent temperature profiles after four heating and cooling cycles, demonstrating excellent photothermal stability (Fig. 4C). Compared to the WEO@BP/GH hydrogel, the BP/GH hydrogel exhibited a comparable photothermal heating capacity (Figs. S7A–C). For example, the central temperature of the BP/GH hydrogel reached 39.5 °C, 54.5 °C, and 68.0 °C at 0.5 W cm^{-2}, 1.0 W cm^{-2}, and 1.5 W cm^{-2} for 5 min, respectively. Moreover, according to the absorbances of samples at 808 nm and plot fitting of samples during the cooling phase, the photothermal conversion efficiency of BP/GH and WEO@BP/GH at

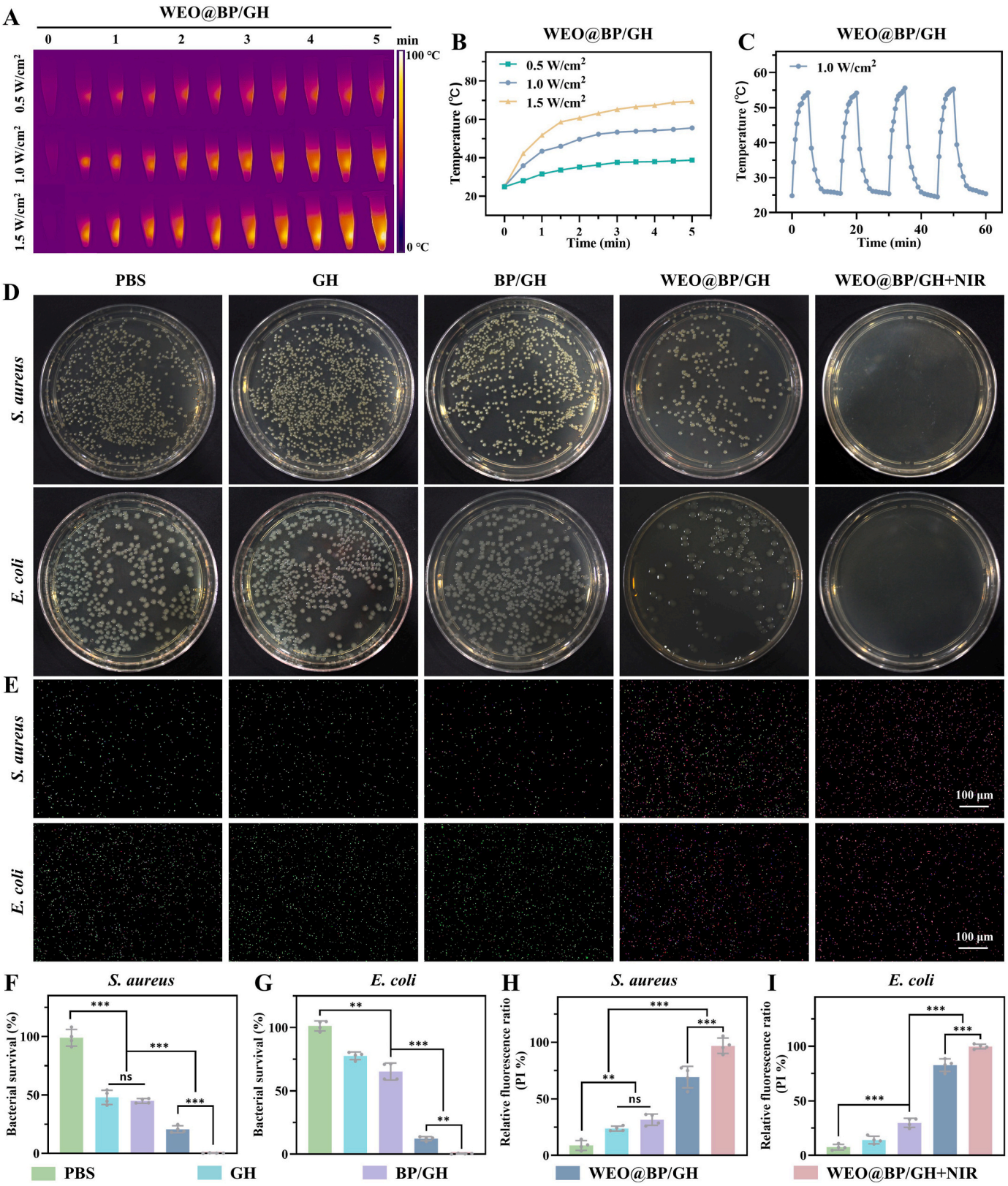

Fig. 4. Antibacterial abilities of the hydrogels in vitro. A) Infrared thermal images of the WEO@BP/GH hydrogel. B) Temperature rise curves of the WEO@BP/GH hydrogel under various NIR power intensities (0.5, 1.0, and 1.5 W/cm^2). C) Photothermal stabilities of the WEO@BP/GH hydrogel under 1.0 W/cm^2 NIR power intensity within four heating and cooling cycles. D) Digital images of the viable *S. aureus* and *E. coli* bacterial clones on agar plates treated with PBS and different hydrogels. E) Live/dead staining of the *S. aureus* and *E. coli* bacteria. Scale bar: 100 μm. F, G) The corresponding bacterial survival ratios of *S. aureus* (F) and *E. coli* (G) were calculated in agar plates. H, I) Quantitative analysis of the relative PI fluorescence ratio of *S. aureus* (H) and *E. coli* (I) in live/dead staining. ns: not significant, $^{**}p < 0.01$, and $^{***}p < 0.001$.

808 nm was calculated as 11.2 % and 7.1 %, respectively (Figs. S8A–C). These results demonstrated that the incorporation of WEO into BP nanosheets had no significant effect on the photothermal performance of BP nanosheets.

Furthermore, these qualities underscore the potential of WEO@BP/GH hydrogels for photothermal-assisted WEO release, which lay the foundation for the WEO@BP/GH dressing to efficiently manipulate the diabetic wound microenvironment for ideal beneficial effects [67,68].

2.2.3. Antibacterial evaluation in vitro

The inflammatory phase starts right after an injury, lasting hours to days in acute wounds, but extending to weeks or months in diabetic wounds due to persistent infection and inflammation [7,69]. Thus, wound dressings are needed to combat drug-resistant bacteria without promoting further resistance [68]. The study shows that BP effectively practices photothermal heating to kill bacteria without inducing resistance. In addition, WEO contains antibacterial compounds like eucalyptol, camphor, trans-chrysanthenol, and terpinyl formate, which work together to target multiple pathways and reduce the risk of drug-resistant bacteria [1,36]. We tested the antibacterial effectiveness of GH, BP/GH, WEO@BP/GH, and WEO@BP/GH + NIR against *S. aureus* and *E. coli*, comparing them to a control group (Fig. 4D). Almost no bacteria colonies grew in the WEO@BP/GH + NIR group. Fig. 4F and G showed that GH group had a survival ratio of 47.9 ± 6.0 % for *S. aureus* and 77.6 % ± 3.1 % for *E. coli*, respectively. Furthermore, the WEO@BP/GH group showed a survival rate of 20.7 % ± 3.0 % for *S. aureus* and 12.3 % ± 1.6 % for *E. coli* due to antibacterial compounds that captured and inactivated pathogens. After NIR irradiation (1.0 W cm^{-2}, 3 min), 99.8 % of both *S. aureus* and *E. coli* were eliminated by the hydrogels. These results indicated that the WEO@BP/GH hydrogels' matrix, which captured bacteria, combined with WEO's antibacterial compounds and BP's photothermal sterilization, provided robust antibacterial activity [28,50].

To additionally investigate the antibacterial effects of WEO@BP/GH hydrogels, a SYTO9/PI live/dead staining assay was performed. SYTO9 stained live bacteria green, while PI labeled dead bacteria red. Fig. 4E showed that most *S. aureus* and *E. coli* treated with PBS displayed green fluorescence, with minimal red fluorescence. The GH group also showed some red fluorescence. In the BP/GH and WEO@BP/GH groups, the red color intensified over time. Following 3 min of NIR irradiation (1.0 W cm^{-2}), the WEO@BP/GH group showed the strongest red fluorescence, indicating a combined antibacterial effect on *S. aureus* and *E. coli*

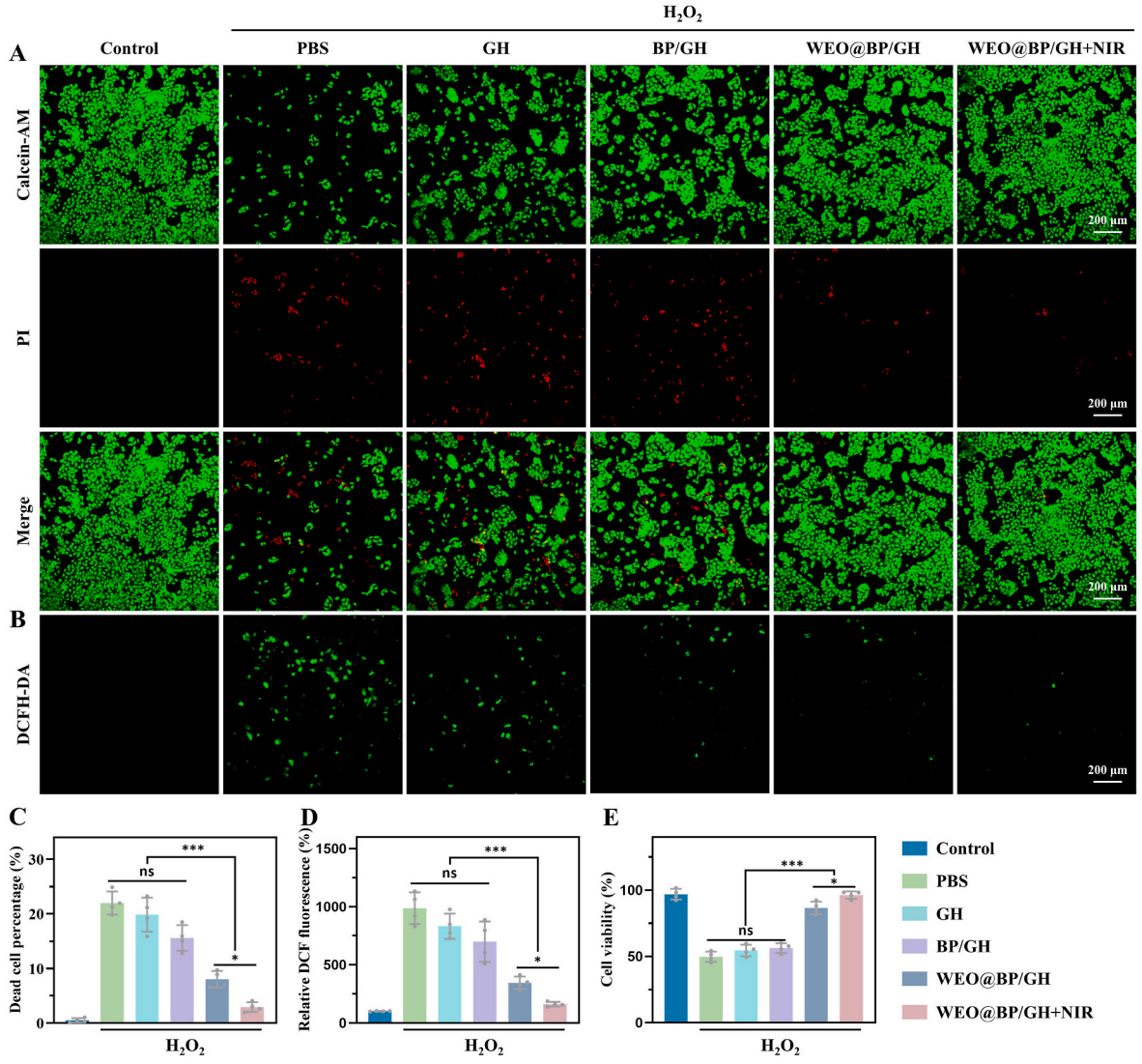

Fig. 5. Antioxidant abilities of the hydrogels in vitro. A, B) Calcein-AM/PI staining (A) and ROS staining (B) of HaCaT cells treated with 500 μM H_2O_2 and different hydrogels. Scale bar: 200 μm. C, D) Quantitative analysis of dead cell percentage (C) and relative DCF fluorescence (D) after treatments with 500 μM H_2O_2 and different hydrogels. E) CCK-8 analysis of the HaCaT cells viability after co-culturing with 500 μM H_2O_2 and different hydrogels. ns: not significant, *$p < 0.05$, and ***$p < 0.001$.

(Fig. 4H and I). Both fluorescence experiments and plate counting tests confirmed similar antibacterial trends, highlighting the potential of WEO@BP/GH hydrogels for antibacterial treatment through the synergy of bacterial capture, antibacterial compounds, and photothermal therapy [70].

2.2.4. Antioxidant performance in vitro

Reactive oxygen species (ROS) play a key role in wound healing, with moderate levels needed to combat damage [8,25]. However, excessive ROS and reduced antioxidants cause redox imbalance, leading to nonhealing diabetic wounds. Thus, managing ROS is vital for controlling inflammation [64,71,72]. After H_2O_2 treatment the HaCaT cells' viabilities were evaluated using live/dead staining. The GH and BP/GH groups showed significantly higher red fluorescence than the WEO@BP/GH and WEO@BP/GH + NIR groups (Fig. 5A and C). Furthermore, we visualized ROS production in HaCaT cells exposed to H_2O_2 using DCFH-DA labeling. Fig. 5B showed fluorescence intensity indicating ROS formation. The WEO@BP/GH hydrogel exhibited lower

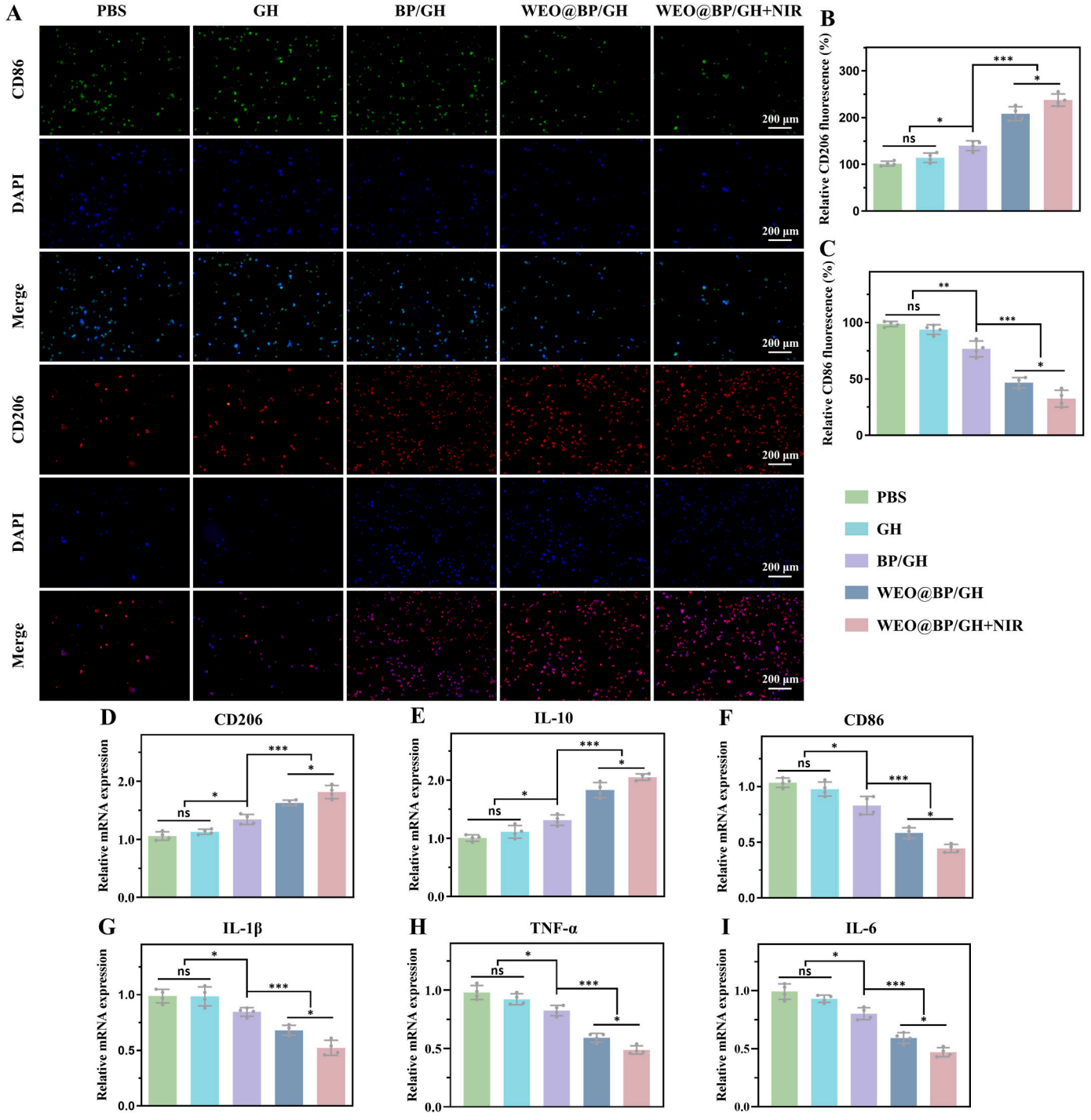

Fig. 6. Anti-inflammation capacities of the hydrogels in vitro. A) Fluorescence microscopic images of CD206 (green) and CD86 (red) in THP-1 cells treated with various samples. B, C) Quantitative analysis of relative fluorescence of CD206 (B) and CD86 (C) in THP-1 cells. D-I) qRT-PCR analysis of the relative mRNA expression of CD206 (D), IL-10 (E), CD86 (F), IL-1β (G), TNF-α (H), and IL-6 (I) in THP-1 cells treated with various samples. ns: not significant, *p < 0.05, **p < 0.01, and ***p < 0.001. (For interpretation of the references to color in this figure legend, the reader is referred to the Web version of this article.)

ROS signals compared to GH and BP/GH hydrogels. Under NIR radiation, the WEO@BP/GH + NIR group had the lowest ROS signals than other groups (Fig. 5D). In addition, The CCK-8 assay showed that WEO-based hydrogels had significantly higher cell viability than other groups when exposed to H_2O_2 (Fig. 5E). These findings suggest that WEO@BP/GH hydrogels have the best effect in removing ROS and providing antioxidant effects under near-infrared (NIR) response. This may be attributed to: (1) The antioxidant properties of polyphenols in wormwood essential oil, such as 5-fluoro-2-hydroxyacetophenone and terpinene, and (2) BP's encapsulation and hydrogel's network structure, which contribute to the controlled release of WEO [1,73]. In addition, these controlled releases of WEO could be enhanced by NIR-triggered temperature increases.

2.2.5. *Anti-inflammation evaluation in vitro*

As integral components of the innate immune system, macrophages perform critical functions in host defense, immune regulation, and wound healing. These adaptable cells demonstrate significant plasticity and can differentiate into various phenotypes, conventionally classified into two categories: the "classically activated" M1 phenotype, which triggers inflammatory responses, and the "alternatively activated" M2 phenotype, which contributes to immunomodulation and tissue

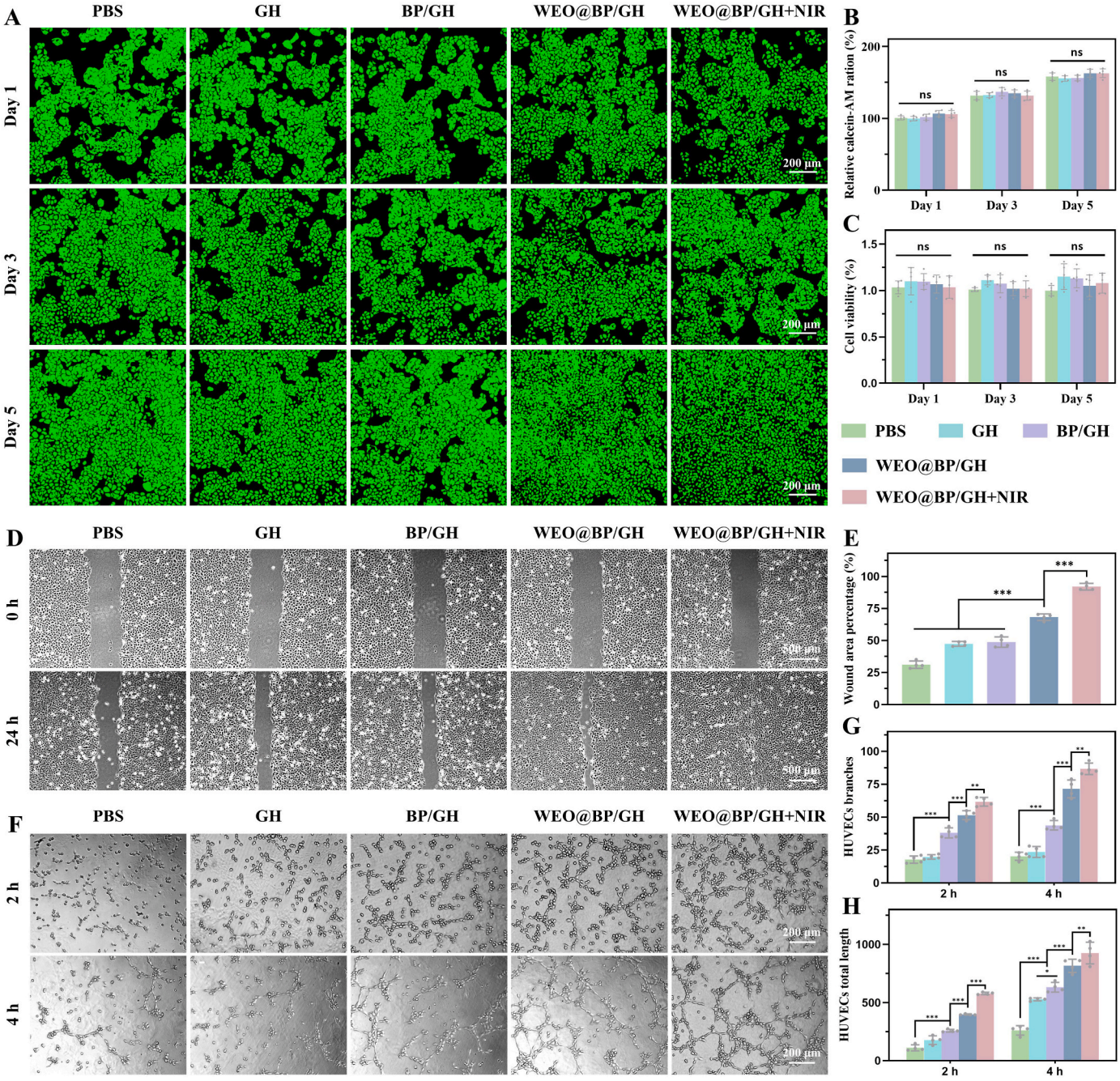

Fig. 7. Cytocompatibility and angiogenic properties of the hydrogels in vitro. A, B) Microscopic images of calcein-AM/PI staining (A) and the quantitative analysis of calcein-AM ration (B) of HaCaT cells treated with PBS and different hydrogels for 1 d, 3 d, and 5 d. Scale bar: 200 μm. C) CCK-8 results of HaCaT cells after co-culturing with PBS and different hydrogels. D) Microscopic images of wound healing using HaCaT cells treated with different hydrogels at 0 and 24 h. Scale bar: 500 μm. E) Quantitative analysis of the wound healing ratios. F) Microscopic images of tube formation using HUVECs treated with different hydrogels at 2 h and 4 h. Scale bar: 200 μm. G, H) Quantitative analysis of the branch points (G) and tube length (H). ns: not significant, *p < 0.05, **p < 0.01, and ***p < 0.001.

remodeling [10,74]. In the context of diabetic wounds, the transition from the M1 to M2 phenotype is impaired, leading to sustained inflammation and delayed wound healing. The presence of phenolic and flavonoid compounds in WEO endows it with immunomodulatory properties [1,75]. Consequently, this study examined the capacity of WEO@BP/GH to promote the polarization of macrophages from the M1 to the M2 phenotype in vitro. The immunofluorescence staining revealed a noticeable elevation in CD206 (a marker of M2 macrophages) and a reduction in CD86 (a marker of M1 macrophages) in WEO@BP/GH + NIR treatment group compared to control group (Fig. 6A–C). Furthermore, RT-PCR analysis revealed a substantial upregulation of M2 markers, specifically CD206 and IL-10, in macrophages co-cultured with WEO@BP/GH + NIR. In contrast, the expression levels of M1 markers, specifically CD86, IL-1β, TNF-α, and IL-6, show a marked reduction (Fig. 6D–I). These findings indicated that WEO@BP/GH hydrogels, when subjected to NIR irradiation, effectively facilitated the polarization of macrophages from the M1 to the M2 phenotype. This transition results in the suppression of pro-inflammatory mediators and the enhancement of anti-inflammatory mediators, thereby advancing the healing process of diabetic wounds [10,62]. The observed anti-inflammatory effects of WEO may be attributed to its ability to inhibit JAK/STAT signaling pathways and scavenge reactive oxygen species, leading to decreased protein and mRNA expression levels of inflammatory factors [76].

2.2.6. Cytocompatibility and angiogenesis assessment in vitro

In clinical settings, hydrogels used for wound dressings must be highly biocompatible [76]. To evaluate this, we performed a leaching assay with HaCaT cells, exposing them to PBS, GH, BP/GH, WEO@BP/GH, and WEO@BP/GH + NIR extraction solutions for 1, 3, and 5 days. Live cells appeared green due to calcein-AM staining, while dead cells were red from propidium iodide (PI) staining. Fluorescence images showed similar green fluorescence intensity across all hydrogel groups compared to the control (Fig. 7A). The relative calcein-AM ratios at 1, 3, and 7 days revealed no significant differences between the groups (Fig. 7B). Additionally, the CCK-8 assay indicated that cell viability in the hydrogel groups exceeded 80 %, demonstrating negligible toxicity of the hydrogels (Fig. 7C).

During the proliferation stage, endothelial and fibroblast cells aid angiogenesis and ECM formation [45,77]. To evaluate WEO-based hydrogels, we conducted scratch tests with HaCaT (Fig. 7D) and tube formation experiments with HUVEC (Fig. 7F) to assess their abilities to enhance fibroblast migration and angiogenesis in vitro. Fig. 7E showed that the WEO@BP/GH group (68.1 ± 2.5 %) had better scratch healing than the PBS group (31.1 ± 2.9 %), GH group (47.4 ± 1.9 %), and BP/GH group (48.7 ± 4.1 %) at 24 h due to the release of WEO. After introducing NIR irradiation, the WEO@BP/GH + NIR group notably exhibited a faster wound healing rate (91.9 ± 2.7 %) at the 24-h mark. To further assess the hydrogel's ability to promote angiogenesis, we tested it with HUVECs (Fig. 7F). At 2 h, the PBS, GH, and BP/GH groups showed minimal tubular structures, while the WEO@BP/GH and WEO@BP/GH + NIR groups displayed more mature and intact formations. By 4 h, the WEO@BP/GH + NIR group had significantly more branch points and longer capillaries, suggesting that NIR-triggered WEO release from the hydrogels enhanced vessel formation (Fig. 7G and H). To have a better validation of the angiogenesis effects of hydrogels, scratch test was also conducted using HUVEC. Similar results were observed that the WEO@BP/GH + NIR group notably exhibited a faster wound healing rate (94.1 ± 1.7 %) at 24 h post-incubation (Figs. S9A–B). The WEO@BP/GH hydrogel's improved cell migration and angiogenesis under NIR irradiation are due to the controlled release of WEO nanoparticles, which reduce oxidative stress barriers and enhance angiogenesis abilities [2,78]. These findings demonstrate that hydrogel does not impede cell migration or angiogenesis, highlighting its excellent biocompatibility alternatively.

2.3. Promoting diabetic wound healing and its mechanism in vivo

Our results in vitro thus far indicate that the WEO@BP/GH hydrogel has effective microenvironment regulation properties, including antibacterial, antioxidant, and angiogenic effects. In addition, these effects could be enhanced due to the NIR-triggered WEO release. Consequently, it is crucial to investigate the impact of WEO@BP/GH hydrogel on wound healing in diabetic rat models in the subsequent phase of research [57,79]. These models enable researchers to replicate the typical wound conditions observed in diabetic patients, assess the hydrogel's efficacy in enhancing wound repair, and examine its effects on various stages of the wound healing process [7,59]. This investigation will contribute to a deeper understanding of the mechanisms underlying diabetic wound healing and offer valuable insights for clinical applications [9].

2.3.1. Diabetic wound healing evaluation in vivo

We evaluated the healing effects of synthesized hydrogels on diabetic rat wounds by creating 8 mm wounds on their backs and treating them with various substances (Fig. 8A). The control group received PBS, while experimental groups were treated with GH, BP/GH, and WEO@BP/GH hydrogels, with one group also exposed to NIR laser irradiation. Wounds were monitored and photographed on days 0, 3, 7, 10, and 14 (Fig. 8B and C). NIR irradiation did not alter the temperature in the control and GH groups. The BP/GH and WEO@BP/GH groups showed a temperature rise, highlighting the photothermal properties of BP nanosheets (Fig. 8D and E). Given the risk of bacterial infection in diabetic wounds, we tested the hydrogels' antibacterial effects in vivo. On day 2, wound secretions were cultured on agar plates. Bacteria were present in samples from the control and GH groups but were scarce in those from the BP/GH and WEO@BP/GH groups. The WEO@BP/GH group showed the highest antimicrobial activity under diabetic conditions (Figs. S10A and B). After three days, the.

WEO@BP/GH + NIR group significantly reduced wound area, achieving a remaining wound area of 30.5 ± 3.8 % after 7 days, outperforming other groups. By day 14, the PBS group still had larger wounds (28.0 ± 1.4 %), while the WEO@BP/GH + NIR group exhibited the best healing, with only 4.9 ± 2.1 % of the wound area remaining (Fig. 8F). Therefore, the WEO@BP/GH hydrogel with 808 nm NIR irradiation proved highly effective for diabetic wound healing.

14 days post-operation, we collected wound and surrounding skin tissues for histological analysis, revealing the hydrogel's effects on diabetic wound healing (Fig. 9A and B). H&E staining indicated nearly complete recovery in WEO@BP/GH + NIR group-treated wounds, with dense granulation tissue and a fully restored epidermis, and scar width reduced to 0.58 ± 0.09 mm (Fig. 9C). In contrast, the PBS group showed crust formation and inflammation. The BP/GH and WEO@BP/GH groups showed underdeveloped granulation tissue and incomplete epidermal bridges, with scar widths of 2.30 ± 0.17 mm and 1.11 ± 0.13 mm. Collagen deposition is vital for cell growth, differentiation, and wound healing [80]. Masson staining revealed that the WEO@BP/GH hydrogel treated with NIR light had collagen fibers aligned parallel to hair follicles, indicating the most orderly collagen deposition (Fig. 9D).

Delayed wound healing is primarily caused by prolonged inflammation. An effective wound dressing should have anti-inflammatory properties [4,81]. After 7 days of PBS treatment, the control group showed more inflammation and fewer blood vessels. In contrast, the GH, BP/GH, and WEO@BP/GH groups showed reduced neutrophils and more blood vessels (Fig. S11A). Notably, the WEO@BP/GH + NIR group exhibited no significant inflammation and numerous blood vessels (Figs. S11B and C). 14 days post-operation, we conducted immunohistochemical staining for myeloperoxidase (MPO) and immunofluorescence staining for Interleukin 6 (IL-6). The PBS group showed the highest MPO and IL-6 expression. In contrast, the GH, BP/GH, WEO@BP/GH, and WEO@BP/GH + NIR groups exhibited progressively lower expression levels, indicating that WEO@BP/GH + NIR treatment

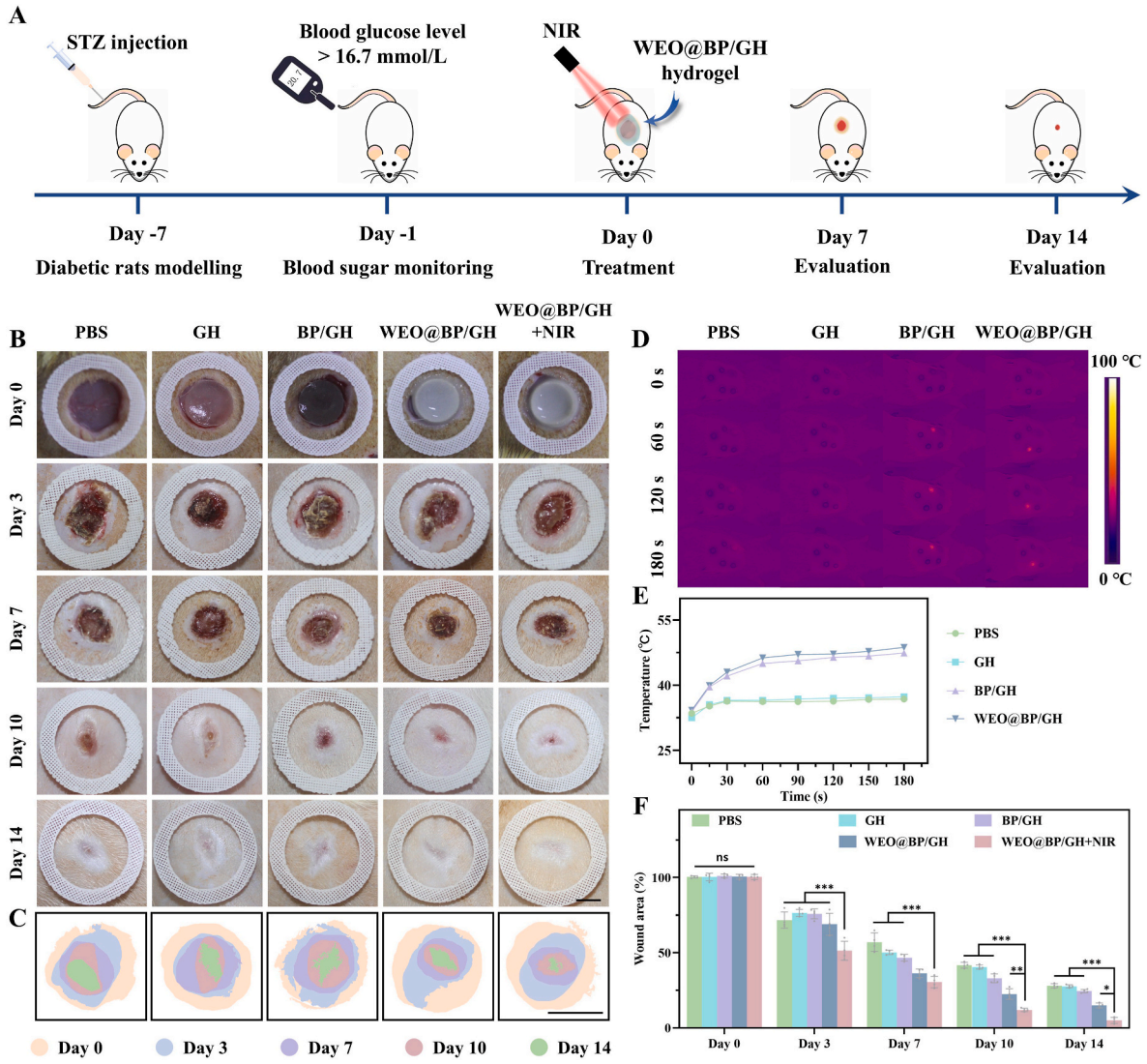

Fig. 8. Diabetic wound healing performance of the hydrogels in vivo. A) Schematic illustration of the diabetic wound modeling, treatment, and evaluation. B) Optical images of the wounds under various treatments on days 0, 3, 7, 10, and 14 (n = 4). Scale bar: 1 mm. C) Schematic diagram of wounds under various treatments on days 0, 3, 7, 10, and 14. Scale bar: 1 mm. D) Infrared thermal images of SD rats under NIR irradiation. E) Temperature rise curves of different groups under NIR irradiation. F) Wound remaining areas of different groups at various time points. ns: not significant, *p < 0.05, **p < 0.01, and ***p < 0.001.

reduced the wound's inflammatory response (Fig. 10A–C, I, and K). To investigate the mechanisms of anti-inflammatory effects, we examined the changes in the macrophages, which were crucial in immune responses to post-tissue injury [74]. Specifically in diabetic wounds, a slow shift from pro-inflammatory (M1) to anti-inflammatory (M2) macrophages hinders tissue healing [20]. Hence, immunofluorescent staining was used to evaluate this, with CD86 marking M1 and CD206 marking M2 macrophages. Fig. 10E, F, M, and N showed that hydrogel-treated groups had a significantly lower percentage of CD86 fluorescence coverage compared to the untreated group, while the fluorescence coverage of CD206 increased. Notably, the WEO@BP/GH + NIR group had the fewest CD86 positive cells and the highest CD206 marker expression. These results suggest that WEO@BP/GH hydrogel with NIR irradiation can accelerate M1 macrophages' transition to M2, thus decreasing inflammation in wounds.

Neovascularization is vital for wound healing, aiding oxygen, nutrient, and immune cell delivery to the injury site, which supports cell growth, collagen production, and re-epithelialization [7,64]. On day 14, immunostaining for CD31 and VEGF, which were used to assess new blood vessels in granulation tissue, revealed faint positive expression in the negative PBS group (Fig. 10B–D, J, and L). Nevertheless, CD31 and VEGF expression increased significantly in the group treated with WEO@BP/GH, especially when exposed to NIR at the injury site. This indicated that WEO@BP/GH + NIR treatment had the strongest angiogenic effect in new skin tissue. The findings showed that WEO@BP/GH hydrogel with NIR irradiation effectively enhances neovascularization in diabetic wounds, aiding the transition from inflammation to repair and remodeling. Besides, the ROS content at the wound site was assessed using DHE staining (Fig. 10G and O). On day 14, the WEO@BP/GH + NIR group showed significantly lower ROS levels (red fluorescence density) compared to other groups, demonstrating the effective in vivo ROS scavenging ability of WEO in the hydrogels with NIR-triggered release. In addition, immunofluorescence staining of MMP-9 to the samples on day 14 was evaluated (Fig. 10H and P). The results showed that the fluorescence level of MMP-9 in the WEO@BP/GH + NIR group was significantly decreased, suggesting that the degradation rate of collagen was slowed down, which could promote the process of wound remodeling and repair.

2.3.2. *Diabetic wound healing mechanisms of WEO@BP/GH hydrogel*

To investigate the underlying effects of the WEO@BP/GH hydrogel, we conducted RNA sequencing analysis on wound tissues obtained from

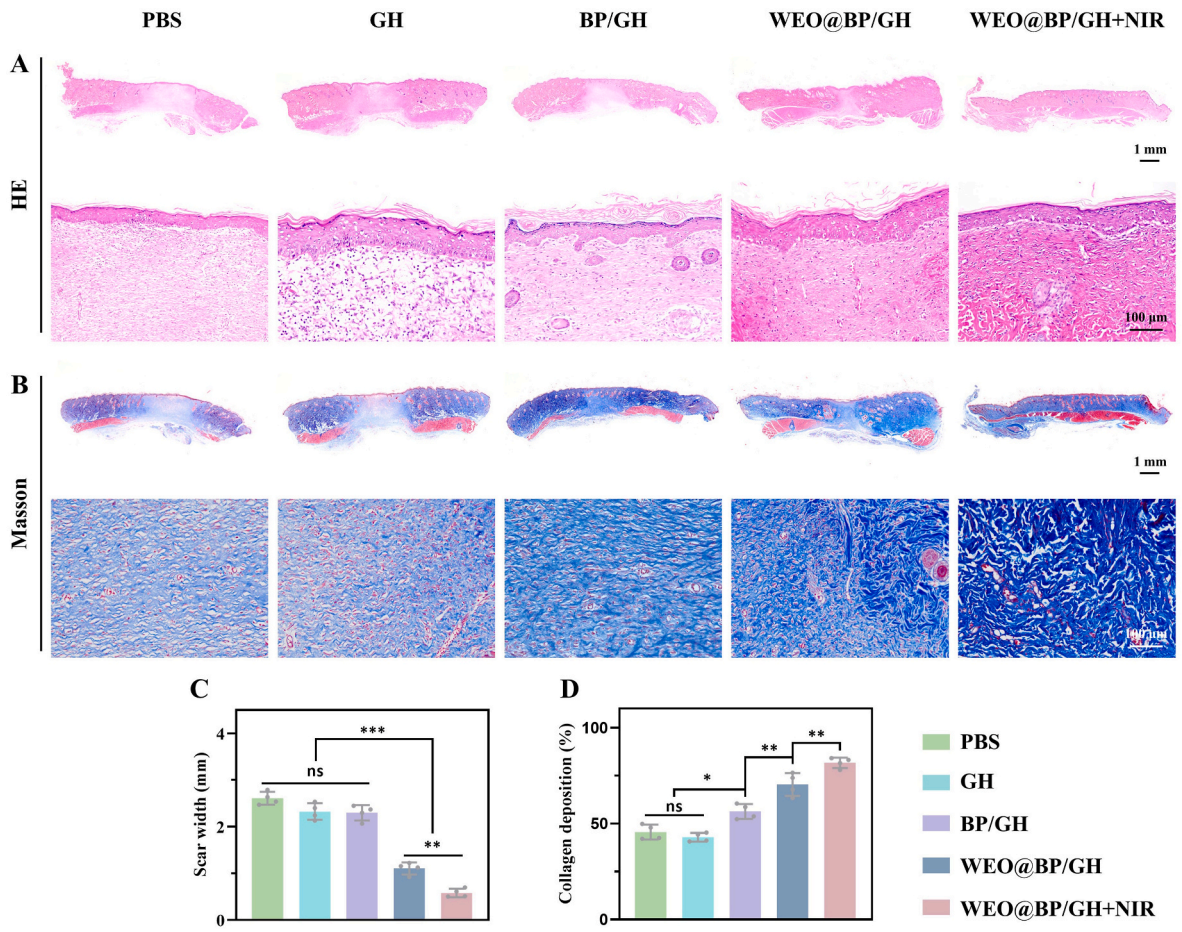

Fig. 9. Histological evaluation of the wound tissues in vivo. A, B) H&E (A) and Masson's trichrome (B) staining of the wound tissues on day 14 after various treatments. Scale bars: 1 mm and 100 μm. C, D) Quantitative analysis of scar width (C) and collagen deposition (D) on day 14 after various treatments. ns: not significant, *p < 0.05, **p < 0.01, and ***p < 0.001.

diabetic rats on day 14 following hydrogel treatment [82]. A total of 30452 genes were found to be co-expressed in tissues from experimental groups. Among these, approximately 20589 genes exhibited differential expression between the control (PBS) group and the WEO@BP/GH + NIR group, while approximately 353 genes showed differential expression with a $|\log_2 FC| \geq 1$ and p-value ≤ 0.05. We utilized GeneCard and OMIM-Gene-Map-Retrieval to retrieve 5517 genes associated with the healing process of diabetic wounds (Fig. 11A). These genes were intersected with differentially expressed genes (DEGs) with $|\log_2 FC| \geq 1$ and p-value ≤ 0.05 between the two groups to obtain 51 intersection genes. Fig. 11B and C displayed the volcano plot and heatmaps of the intersection genes. The intersection genes were further examined through protein-protein interaction (PPI) network analysis (Fig. 11D). The size of each node in the PPI network indicated the strength of their association with other protein molecules. The PPI network results identified key signaling molecules involved in inflammation regulation and cell migration promotion, including IL1B, LEP, MMP13, and IL1A [82]. Kyoto Encyclopedia of Genes and Genomes (KEGG) pathway enrichment analysis of the 51 intersection genes (Fig. 11E) showed that those genes were significantly enriched in cytokine-cytokine receptor interaction, IL-17 signaling pathway, NF-kappa B signaling pathway, TNF signaling pathway, and AMPK signaling pathway [83]. This observation served as a reminder that the combination of WEO@BP/GH hydrogel and NIR irradiation may potentially reduce inflammatory.response, regulate immune response, and promote angiogenesis in the mechanisms of promoting diabetic wound healing. Subsequently, a Gene Ontology (GO) enrichment analysis was conducted (Fig. 11F and G). The analysis revealed several significantly enriched biological processes, including regulation of inflammatory response, positive regulation of interleukin-6 and interleukin-8 production, and positive regulation of vascular endothelial growth factor production. The findings depicted in Figs. 7 and 10 demonstrated that following treatment with WEO@BP/GH + NIR, there was an increase in cell migration rate, angiogenesis, and a decrease in the positive rate of IL-6 immunofluorescence staining, which aligns with the transcriptome data.

2.3.3. *Biosafety evaluation in vivo*

Finally, the biosafety assessment of the synthesized hydrogels was conducted to ascertain their suitability for application in diabetic wound healing [84]. Firstly, the in vitro degradation properties of BP were evaluated (Figs. S12A–C). Through observing the optical change of the black phosphorus solution with the extension of time, we found that the color of the solution gradually became lighter, indicating that the black phosphorus gradually degraded. Furthermore, we detected the phosphate content in the supernatant of black phosphorus. Results exhibited that the phosphate content gradually increased with the extension of time and the increase rate was accelerated under NIR irradiation. These results indicated that black phosphorus could be degraded into non-toxic phosphate in aqueous solution. As illustrated in Fig. S13A, major organs, including the heart, liver, spleen, lung, and kidney, were harvested from rats 14 days post-operation and subjected to HE staining. The results indicated an absence of significant pathological abnormalities or damage in these organs across all experimental groups. Furthermore, blood biochemical analyses and blood routine examination revealed no significant deviations in any parameters between the treated groups and the control group (Figs. S13B–I). Based on these

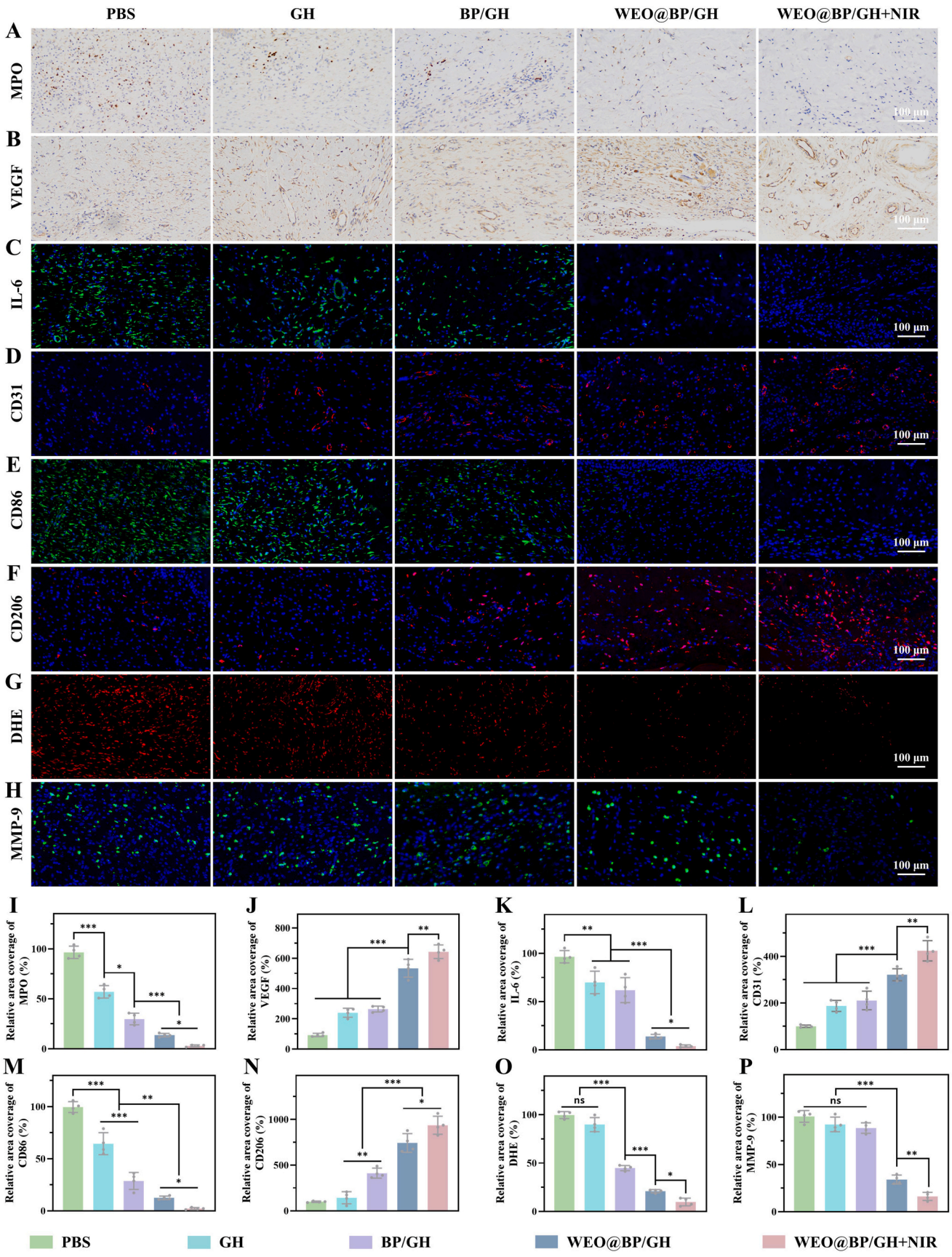

Fig. 10. Immunohistochemical and immunofluorescence staining of the wound tissues in vivo. A, B) Immunohistochemical staining of MPO (A) and VEGF (B) in tissue sections on day 14. Scale bar: 100 μm. C-H) Immunofluorescence staining of IL-6 (C), CD31 (D), CD86 (E), CD206 (F), DHE (G), and MMP-9 (H) in tissue sections on day 14. Scale bar: 100 μm. I-P) Quantitative analysis of MPO (I), VEGF (J), IL-6 (K), CD31 (L), CD86 (M), CD206 (N), DHE (O), and MMP-9 (P) in tissue sections on day 14. ns: not significant, *$p < 0.05$, **$p < 0.01$, and ***$p < 0.001$.

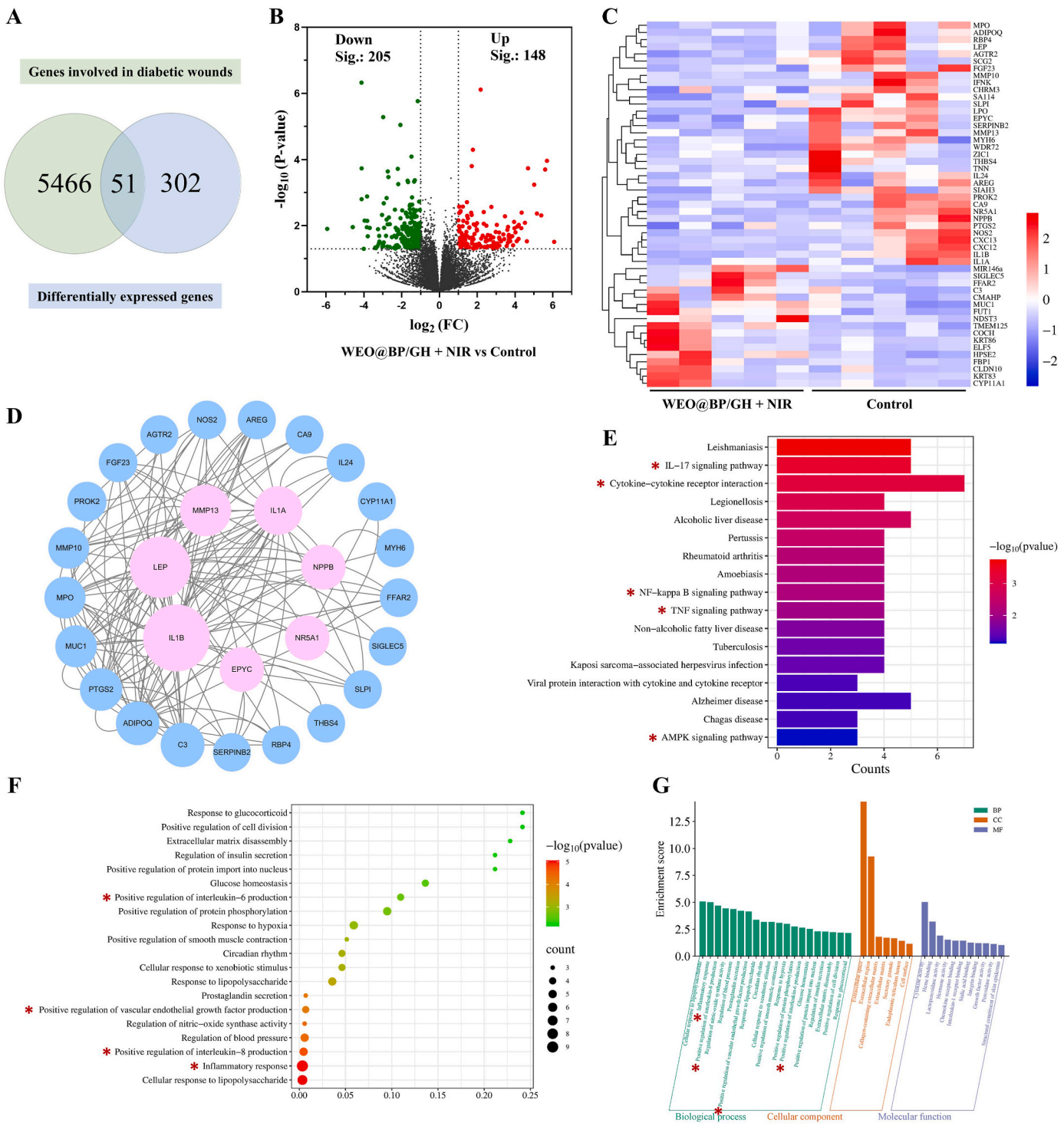

Fig. 11. Diabetic wound healing mechanisms. A) Venn diagram of the differential gene counts in WEO@BP/GH + NIR group, control group, and diabetic wound healing. B, C) The volcano plot (B) and heatmap (C) of the significantly differentially expressed genes in wound sites after WEO@BP/GH + NIR treatment relative to the control group. D) Protein-protein interaction network of the significantly differentially expressed genes. E, F) KEGG pathway enrichment evaluation. G) GO enrichment analysis of the differentially expressed genes.

results, it is evident that these hydrogels have great potential for clinical application.

3. Conclusion

In summary, we have effectively engineered a highly promising multifunctional hydrogel, designated as WEO@BP/GH, which integrates WEO@BP nanoparticles with a biocompatible GelMA/HAMA hydrogel matrix, exhibiting robust microenvironmental regulatory properties. The incorporation of bio-friendly BP nanosheets significantly enhances the encapsulation stability of WEO and augments the hydrogel's microenvironmental regulation capabilities through the NIR-triggered release of WEO. Comprehensive in vitro and in vivo experiments have demonstrated that the WEO@BP/GH hydrogels play a crucial regulatory role in four key areas, including: 1) Remarkable synergistic antibacterial effects attributed to the antibacterial

compounds in WEO and the photothermal properties of BP nanosheets. 2) Outstanding antioxidant capacities through efficient scavenging of ROS. 3) Effective anti-inflammatory capabilities by modulating the M1/M2 macrophage ratio. 4) Enhancing angiogenic properties through WEO-associated vasotropic components, thereby accelerating vascular regeneration. Collectively, this strategy presents significant potential as an ideal therapeutic approach for promoting the healing of diabetic wounds.

4. Experimental section

The Supplementary date contains all materials and methods.

CRediT authorship contribution statement

Mengjuan Tao: Writing – original draft, Methodology, Formal analysis, Data curation. **Zhiwei Sun:** Writing – original draft, Visualization, Validation, Methodology. **Haiyan Wang:** Software, Resources, Investigation. **Na Meng:** Validation, Software, Methodology, Formal analysis. **Xiangru Chen:** Investigation, Conceptualization. **Jianwei Mao:** Visualization, Investigation. **Heyan Huang:** Software, Investigation. **Yan Huang:** Visualization, Investigation. **Jin Liu:** Software, Resources. **Zhenxing Wang:** Software, Methodology. **Weiqiang Tan:** Investigation, Data curation. **Yonggang Chen:** Supervision, Project administration, Methodology, Conceptualization. **Chuchao Zhou:** Writing – review & editing, Supervision, Project administration, Funding acquisition. **Yanqing Yang:** Writing – review & editing, Supervision, Resources, Project administration, Funding acquisition.

Declaration of competing interest

The authors declare no conflict of interest.

Acknowledgment

This work was supported by the Hubei Provincial Central Guidance Local Science and Technology Development Project (2022BGE264), Health Commission of Hubei Provincial (WJ2023Q017, WJ2023M130), and Knowledge Innovation Project of Wuhan (2023020201020546).

Appendix A. Supplementary data

Supplementary data to this article can be found online at https://doi.org/10.1016/j.mtbio.2025.101751.

Data availability

Data will be made available on request.

References

[1] F. Wang, Q. Sun, Y. Li, R. Xu, R. Li, D. Wu, R. Huang, Z. Yang, Y. Li, Hydrogel encapsulating wormwood essential oil with broad-spectrum antibacterial and immunomodulatory properties for infected diabetic wound healing, Adv. Sci. 11 (3) (2024) e2305078, https://doi.org/10.1002/advs.202305078.

[2] N. Meng, C. Zhou, Z. Sun, X. Chen, S. Xiong, M. Tao, Y. Qin, K. Hu, L. Ma, D. Tian, F. Zhu, Y. Yang, Tailored gelatin methacryloyl-based hydrogel with near-infrared responsive delivery of qiai essential oils boosting reactive oxygen species scavenging, antimicrobial, and anti-inflammatory activities for diabetic wound healing, Int. J. Biol. Macromol. 263 (Pt 2) (2024) 130386, https://doi.org/10.1016/j.ijbiomac.2024.130386.

[3] X. Qi, E. Cai, Y. Xiang, C. Zhang, X. Ge, J. Wang, Y. Lan, H. Xu, R. Hu, J. Shen, An immunomodulatory hydrogel by hyperthermia-assisted self-cascade glucose depletion and ros scavenging for diabetic foot ulcer wound therapeutics, Adv. Mater. 35 (48) (2023) e2306632, https://doi.org/10.1002/adma.202306632.

[4] A.U.R. Khan, K. Huang, M.S. Khalaji, F. Yu, X. Xie, T. Zhu, Y. Morsi, Z. Jinzhong, X. Mo, Multifunctional bioactive core-shell electrospun membrane capable to terminate inflammatory cycle and promote angiogenesis in diabetic wound, Bioact. Mater. 6 (9) (2021) 2783–2800, https://doi.org/10.1016/j.bioactmat.2021.01.040.

[5] Q. Bai, K. Han, K. Dong, C. Zheng, Y. Zhang, Q. Long, T. Lu, Potential applications of nanomaterials and technology for diabetic wound healing, Int. J. Nanomed. 15 (2020) 9717–9743, https://doi.org/10.2147/IJN.S276001.

[6] M. Chang, T.T. Nguyen, Strategy for treatment of infected diabetic foot ulcers, Accounts Chem. Res. 54 (5) (2021) 1080–1093, https://doi.org/10.1021/acs.accounts.0c00864.

[7] S. Zhu, B. Zhao, M. Li, H. Wang, J. Zhu, Q. Li, H. Gao, Q. Feng, X. Cao, Microenvironment responsive nanocomposite hydrogel with nir photothermal therapy, vascularization and anti-inflammation for diabetic infected wound healing, Bioact. Mater. 26 (2023) 306–320, https://doi.org/10.1016/j.bioactmat.2023.03.005.

[8] L. Deng, C. Du, P. Song, T. Chen, S. Rui, D.G. Armstrong, W. Deng, The role of oxidative stress and antioxidants in diabetic wound healing, Oxid. Med. Cell. Longev. 2021 (2021) 8852759, https://doi.org/10.1155/2021/8852759.

[9] Z. Shao, T. Yin, J. Jiang, Y. He, T. Xiang, S. Zhou, Wound microenvironment self-adaptive hydrogel with efficient angiogenesis for promoting diabetic wound healing, Bioact. Mater. 20 (2023) 561–573, https://doi.org/10.1016/j.bioactmat.2022.06.018.

[10] Y. Qian, Y. Zheng, J. Jin, X. Wu, K. Xu, M. Dai, Q. Niu, H. Zheng, X. He, J. Shen, Immunoregulation in diabetic wound repair with a photoenhanced glycyrrhizic acid hydrogel scaffold, Adv. Mater. 34 (29) (2022) e2200521, https://doi.org/10.1002/adma.202200521.

[11] C. Guo, Y. Wu, W. Li, Y. Wang, Q. Kong, Development of a microenvironment-responsive hydrogel promoting chronically infected diabetic wound healing through sequential hemostatic, antibacterial, and angiogenic activities, ACS Appl. Mater. Interfaces 14 (27) (2022) 30480–30492, https://doi.org/10.1021/acsami.2c02725.

[12] W. Fan, H. Lu, H. Shi, W. Yuan, G. Liu, Trends and challenges on inflammatory microenvironment in diabetic wound from 2014 to 2023: a bibliometric analysis, Int. Wound J. 21 (8) (2024) e14913, https://doi.org/10.1111/iwj.14913.

[13] M. Shi, Z. Du, Y. Qi, W. Li, H. Hu, X. Lin, S. Wang, Z. Tang, M. Zhou, Wound microenvironment-responsive glucose consumption and hydrogen peroxide generation synergistic with azithromycin for diabetic wounds healing, Theranostics 12 (6) (2022) 2658–2673, https://doi.org/10.7150/thno.64244.

[14] Y. Liang, J. He, B. Guo, Functional hydrogels as wound dressing to enhance wound healing, ACS Nano 15 (8) (2021) 12687–12722, https://doi.org/10.1021/acsnano.1c04206.

[15] Z. Arabpour, F. Abedi, M. Salehi, S.M. Baharnoori, M. Soleimani, A.R. Djalilian, Hydrogel-based skin regeneration, Int. J. Mol. Sci. 25 (4) (2024), https://doi.org/10.3390/ijms25041982.

[16] C. Jian, M. Wang, Y. Qian, X. Song, L. Wang, L. Li, L. Huang, G. Wang, X. Shi, J. Dong, H. Li, A. Lin, L. Shi, A tlr4-targeting bioactive peptide hydrogel to regulate immune-microenvironment for diabetic wound repair, Adv. Healthcare Mater. 13 (19) (2024) e2400391, https://doi.org/10.1002/adhm.202400391.

[17] E.I. Oprita, A. Iosageanu, O. Craciunescu, Natural polymeric hydrogels encapsulating small molecules for diabetic wound healing, Gels 9 (11) (2023), https://doi.org/10.3390/gels9110867.

[18] W. Yuan, C. Huang, W. Deng, J. Lai, J. Chen, J. Jie, Y. Wu, T. You, L.P. Wu, Hyaluronic acid methacryloyl/chitosan methacryloyl/3-methacrylamidophenylboronic acid multifunctional hydrogel loading exosome for diabetic wound healing, Int. J. Biol. Macromol. 280 (Pt 3) (2024) 135562, https://doi.org/10.1016/j.ijbiomac.2024.135562.

[19] Z. Ma, W. Song, Y. He, H. Li, Multilayer injectable hydrogel system sequentially delivers bioactive substances for each wound healing stage, ACS Appl. Mater. Interfaces 12 (26) (2020) 29787–29806, https://doi.org/10.1021/acsami.0c06360.

[20] H. Zhao, J. Huang, Y. Li, X. Lv, H. Zhou, H. Wang, Y. Xu, C. Wang, J. Wang, Z. Liu, Ros-scavenging hydrogel to promote healing of bacteria infected diabetic wounds, Biomaterials 258 (2020) 120286, https://doi.org/10.1016/j.biomaterials.2020.120286.

[21] B. Zeng, Z. Mu, T. Shen, X. Qi, Y. Chen, K. Lei, C. Huang, Y. Wang, R. Hu, X. Cai, J. Shen, H. Deng, A self-propelled nanovesicle with robust antibacterial and regeneration-promoting capabilities for treating biofilm-induced periodontitis, Chin. Chem. Lett. (2024) 110350, https://doi.org/10.1016/j.cclet.2024.110350.

[22] J. Chen, Z. Mu, D. Chen, C. Huang, T. Jin, L. Li, Y. Zeng, Q. Zhou, Y. Zhang, H. Mao, H. Deng, X. Shen, H. Yang, X. Cai, H2s-releasing versatile hydrogel dressing with potent antimicrobial, anti-inflammatory, epithelialization and angiogenic capabilities for diabetic wound healing, Chemical engineering journal (Lausanne, Switzerland : 1996) 469 (2023) 143985, https://doi.org/10.1016/j.cej.2023.143985.

[23] L. Li, D. Chen, J. Chen, C. Yang, Y. Zeng, T. Jin, Y. Zhang, X. Sun, H. Mao, Z. Mu, X. Shen, Z. Ruan, X. Cai, Gelatin and catechol-modified quaternary chitosan cotton dressings with rapid hemostasis and high-efficiency antimicrobial capacity to manage severe bleeding wounds, Mater. Des. 229 (2023) 111927, https://doi.org/10.1016/j.matdes.2023.111927.

[24] C. Tu, H. Lu, T. Zhou, W. Zhang, L. Deng, W. Cao, Z. Yang, Z. Wang, X. Wu, J. Ding, F. Xu, C. Gao, Promoting the healing of infected diabetic wound by an anti-bacterial and nano-enzyme-containing hydrogel with inflammation-suppressing, ros-scavenging, oxygen and nitric oxide-generating properties, Biomaterials 286 (2022) 121597, https://doi.org/10.1016/j.biomaterials.2022.121597.

[25] Y. Kang, L. Xu, J. Dong, X. Yuan, J. Ye, Y. Fan, B. Liu, J. Xie, X. Ji, Programmed microalgae-gel promotes chronic wound healing in diabetes, Nat. Commun. 15 (1) (2024) 1042, https://doi.org/10.1038/s41467-024-45101-9.

[26] J.C. Borges, L.A. de Almeida Campos, E.A.M. Kretzschmar, I.M.F. Cavalcanti, Incorporation of essential oils in polymeric films for biomedical applications, Int. J.

Biol. Macromol. 269 (Pt 1) (2024) 132108, https://doi.org/10.1016/j.ijbiomac.2024.132108.
[27] M. Sathuvan, R. Thangam, K.L. Cheong, H. Kang, Y. Liu, Kappa-carrageenan-essential oil loaded composite biomaterial film facilitates mechanosensing and tissue regenerative wound healing, Int. J. Biol. Macromol. 241 (2023) 124490, https://doi.org/10.1016/j.ijbiomac.2023.124490.
[28] Y. Qiu, T. Yang, H. Zhang, H. Dai, H. Gao, W. Feng, D. Xu, J. Duan, The application of ph-responsive hyaluronic acid-based essential oils hydrogels with enhanced anti-biofilm and wound healing, Int. J. Biol. Macromol. 275 (Pt 2) (2024) 133559, https://doi.org/10.1016/j.ijbiomac.2024.133559.
[29] S. Perteghella, A. Garzoni, A. Invernizzi, M. Sorrenti, C. Boselli, A. Icaro Cornaglia, D. Dondi, S. Lazzaroni, G. Marrubini, C. Caramella, L. Catenacci, M.C. Bonferoni, Nanoemulsions of clove oil stabilized with chitosan oleate-antioxidant and wound-healing activity, Antioxidants 12 (2) (2023) 273, https://doi.org/10.3390/antiox12020273.
[30] U. Zagorc, D. Bozic, V. Arrigler, Z. Medos, M. Hocevar, A. Romolo, V. Kralj-Iglic, K. Kogej, The effect of different surfactants and polyelectrolytes on nano-vesiculation of artificial and cellular membranes, Molecules 29 (19) (2024), https://doi.org/10.3390/molecules29194590.
[31] Y. Jia, X. Zhai, W. Fu, Y. Liu, F. Li, C. Zhong, Surfactant-free emulsions stabilized by tempo-oxidized bacterial cellulose, Carbohydr. Polym. 151 (2016) 907–915, https://doi.org/10.1016/j.carbpol.2016.05.099.
[32] D. Qiu, C. Zheng, Y. Zeng, L. Wu, C. Huang, Y. Ran, Y. Ding, J. Shi, X. Cai, Y. Pan, Enzymolysis and photothermal-mediated synergistic antimicrobial nanoplatform with programmed eps degradation and biofilm penetration capabilities for eradication of biofilm wound infections, Chemical engineering journal (Lausanne, Switzerland: 1996) 477 (2023) 147217, https://doi.org/10.1016/j.cej.2023.147217.
[33] Z. Mu, T. Jin, T. Chu, H. Lu, Y. Chen, S. Li, B. Zeng, C. Huang, K. Lei, X. Cai, H. Deng, R. Hu, Functionalized mos2-nanosheets with nir-triggered nitric oxide delivery and photothermal activities for synergistic antibacterial and regeneration-promoting therapy, J. Nanobiotechnol. 21 (1) (2023) 1–463, https://doi.org/10.1186/s12951-023-02167-9.
[34] X. Chen, Z. Sun, X. Peng, N. Meng, L. Ma, J. Fu, J. Chen, Y. Liu, Y. Yang, C. Zhou, Graphene oxide/black phosphorus functionalized collagen scaffolds with enhanced near-infrared controlled in situ biomineralization for promoting infectious bone defect repair through pi3k/akt pathway, ACS Appl. Mater. Interfaces 16 (38) (2024) 50369–50388, https://doi.org/10.1021/acsami.4c10284.
[35] C. Xue, L. Sutrisno, M. Li, W. Zhu, Y. Fei, C. Liu, X. Wang, K. Cai, Y. Hu, Z. Luo, Implantable multifunctional black phosphorus nanoformulation-deposited biodegradable scaffold for combinational photothermal/chemotherapy and wound healing, Biomaterials 269 (2021) 120623, https://doi.org/10.1016/j.biomaterials.2020.120623.
[36] J. Ouyang, X. Ji, X. Zhang, C. Feng, Z. Tang, N. Kong, A. Xie, J. Wang, X. Sui, L. Deng, Y. Liu, J.S. Kim, Y. Cao, W. Tao, In situ sprayed nir-responsive, analgesic black phosphorus-based gel for diabetic ulcer treatment, Proc. Natl. Acad. Sci. 117 (46) (2020) 28667–28677, https://doi.org/10.1073/pnas.2016268117.
[37] Q. Ding, T. Sun, W. Su, X. Jing, B. Ye, Y. Su, L. Zeng, Y. Qu, X. Yang, Y. Wu, Z. Luo, X. Guo, Bioinspired multifunctional black phosphorus hydrogel with antibacterial and antioxidant properties: a stepwise countermeasure for diabetic skin wound healing, Adv. Healthcare Mater. 11 (12) (2022) e2102791, https://doi.org/10.1002/adhm.202102791.
[38] M. Cui, J. Zhang, P. Han, L. Shi, X. Li, Z. Zhang, H. Bao, Y. Ma, Z. Tao, X. Dong, L. Fu, Y. Wu, Two-dimensional nanomaterials: a multifunctional approach for robust for diabetic wound repair, Mater Today Bio 28 (2024) 101186, https://doi.org/10.1016/j.mtbio.2024.101186.
[39] C. Geng, S. He, S. Yu, H.M. Johnson, H. Shi, Y. Chen, Y.K. Chan, W. He, M. Qin, X. Li, Y. Deng, Achieving clearance of drug-resistant bacterial infection and rapid cutaneous wound regeneration using an ros-balancing-engineered heterojunction, Adv. Mater. 36 (16) (2024) e2310599, https://doi.org/10.1002/adma.202310599.
[40] A. Maleki, J. He, S. Bochani, V. Nosrati, M.A. Shahbazi, B. Guo, Multifunctional photoactive hydrogels for wound healing acceleration, ACS Nano 15 (12) (2021) 18895–18930, https://doi.org/10.1021/acsnano.1c08334.
[41] D. Simões, S.P. Miguel, M.P. Ribeiro, P. Coutinho, A.G. Mendonça, I.J. Correia, Recent advances on antimicrobial wound dressing: a review, Eur. J. Pharm. Biopharm. 127 (2018) 130–141, https://doi.org/10.1016/j.ejpb.2018.02.022.
[42] H. Hu, F.J. Xu, Rational design and latest advances of polysaccharide-based hydrogels for wound healing, Biomater. Sci. 8 (8) (2020) 2084–2101, https://doi.org/10.1039/d0bm00055h.
[43] T. Kolipaka, G. Pandey, N. Abraham, D.A. Srinivasarao, R.S. Raghuvanshi, P. S. Rajinikanth, V. Tickoo, S. Srivastava, Stimuli-responsive polysaccharide-based smart hydrogels for diabetic wound healing: design aspects, preparation methods and regulatory perspectives, Carbohydr. Polym. 324 (2024) 121537, https://doi.org/10.1016/j.carbpol.2023.121537.
[44] Z. Sun, K. Hu, T. Wang, X. Chen, N. Meng, X. Peng, L. Ma, D. Tian, S. Xiong, C. Zhou, Y. Yang, Enhanced physiochemical, antibacterial, and hemostatic performance of collagen-quaternized chitosan-graphene oxide sponges for promoting infectious wound healing, Int. J. Biol. Macromol. 266 (Pt 2) (2024) 131277, https://doi.org/10.1016/j.ijbiomac.2024.131277.
[45] K. Zha, W. Zhang, W. Hu, M. Tan, S. Zhang, Y. Yu, S. Gou, P. Bu, B. Zhou, Y. Zou, Y. Xiong, B. Mi, G. Liu, Q. Feng, K. Cai, Three-step regenerative strategy: multifunctional bilayer hydrogel for combined photothermal/photodynamic therapy to promote drug-resistant bacteria-infected wound healing, Adv. Funct. Mater. 34 (2) (2024), https://doi.org/10.1002/adfm.202308145.
[46] Z. Li, X. Xing, C. Zhao, Q. Wu, J. Liu, X. Qiu, L. Wang, A rapid interactive chitosan-based medium with antioxidant and pro-vascularization properties for infected burn wound healing, Carbohydr. Polym. 333 (2024) 121991, https://doi.org/10.1016/j.carbpol.2024.121991.
[47] A. Dev, S.J. Mohanbhai, A.C. Kushwaha, A. Sood, M.N. Sardoiwala, S. R. Choudhury, S. Karmakar, Kappa-carrageenan-c-phycocyanin based smart injectable hydrogels for accelerated wound recovery and real-time monitoring, Acta Biomater. 109 (2020) 121–131, https://doi.org/10.1016/j.actbio.2020.03.023.
[48] Z. Zhou, T. Deng, M. Tao, L. Lin, L. Sun, X. Song, D. Gao, J. Li, Z. Wang, X. Wang, J. Li, Z. Jiang, L. Luo, L. Yang, M. Wu, Snail-inspired afg/gelma hydrogel accelerates diabetic wound healing via inflammatory cytokines suppression and macrophage polarization, Biomaterials 299 (2023) 122141, https://doi.org/10.1016/j.biomaterials.2023.122141.
[49] L. Xue, T. Deng, R. Guo, L. Peng, J. Guo, F. Tang, J. Lin, S. Jiang, H. Lu, X. Liu, L. Deng, A composite hydrogel containing mesoporous silica nanoparticles loaded with artemisia argyi extract for improving chronic wound healing, Front. Bioeng. Biotechnol. 10 (2022) 825339, https://doi.org/10.3389/fbioe.2022.825339.
[50] Z. Sun, X. Chen, F. Miao, N. Meng, K. Hu, S. Xiong, X. Peng, L. Ma, C. Zhou, Y. Yang, Engineering ag-decorated graphene oxide nano-photothermal platforms with enhanced antibacterial properties for promoting infectious wound healing, Int. J. Nanomed. 19 (2024) 8901–8927, https://doi.org/10.2147/IJN.S474536.
[51] J. Ruan, X. Wang, Z. Yu, Z. Wang, Q. Xie, D. Zhang, Y. Huang, H. Zhou, X. Bi, C. Xiao, P. Gu, X. Fan, Enhanced physiochemical and mechanical performance of chitosan-grafted graphene oxide for superior osteoinductivity, Adv. Funct. Mater. 26 (7) (2016) 1085–1097, https://doi.org/10.1002/adfm.201504141.
[52] Y. Zhao, C. Tian, Y. Liu, Z. Liu, J. Li, Z. Wang, X. Han, All-in-one bioactive properties of photothermal nanofibers for accelerating diabetic wound healing, Biomaterials 295 (2023) 122029, https://doi.org/10.1016/j.biomaterials.2023.122029.
[53] B. Guo, R. Dong, Y. Liang, M. Li, Haemostatic materials for wound healing applications, Nature reviews, Chemistry 5 (11) (2021) 773–791, https://doi.org/10.1038/s41570-021-00323-z.
[54] X. Han, C. Saengow, L. Ju, W. Ren, R.H. Ewoldt, J. Irudayaraj, Exosome-coated oxygen nanobubble-laden hydrogel augments intracellular delivery of exosomes for enhanced wound healing, Nat. Commun. 15 (1) (2024) 3435, https://doi.org/10.1038/s41467-024-47696-5.
[55] B. Guo, Y. Liang, R. Dong, Physical dynamic double-network hydrogels as dressings to facilitate tissue repair, Nat. Protoc. 18 (11) (2023) 3322–3354, https://doi.org/10.1038/s41596-023-00878-9.
[56] W. Zhang, B. Bao, F. Jiang, Y. Zhang, R. Zhou, Y. Lu, S. Lin, Q. Lin, X. Jiang, L. Zhu, Promoting oral mucosal wound healing with a hydrogel adhesive based on a phototriggered s-nitrosylation coupling reaction, Adv. Mater. 33 (48) (2021) e2105667, https://doi.org/10.1002/adma.202105667.
[57] Y. Li, R. Fu, Z. Duan, C. Zhu, D. Fan, Artificial nonenzymatic antioxidant mxene nanosheet-anchored injectable hydrogel as a mild photothermal-controlled oxygen release platform for diabetic wound healing, ACS Nano 16 (5) (2022) 7486–7502, https://doi.org/10.1021/acsnano.1c10575.
[58] Y. Jiang, A.A. Trotsyuk, S. Niu, D. Henn, K. Chen, C.C. Shih, M.R. Larson, A. M. Mermin-Bunnell, S. Mittal, J.C. Lai, A. Saberi, E. Beard, S. Jing, D. Zhong, S. R. Steele, K. Sun, T. Jain, E. Zhao, C.R. Neimeth, W.G. Viana, J. Tang, D. Sivaraj, J. Padmanabhan, M. Rodrigues, D.P. Perrault, A. Chattopadhyay, Z.N. Maan, M. C. Leeolou, C.A. Bonham, S.H. Kwon, H.C. Kussie, K.S. Fischer, G. Gurusankar, K. Liang, K. Zhang, R. Nag, M.P. Snyder, M. Januszyk, G.C. Gurtner, Z. Bao, Wireless, closed-loop, smart bandage with integrated sensors and stimulators for advanced wound care and accelerated healing, Nat. Biotechnol. 41 (5) (2023) 652–662, https://doi.org/10.1038/s41587-022-01528-3.
[59] Y. Xiong, Z. Lin, P. Bu, T. Yu, Y. Endo, W. Zhou, Y. Sun, F. Cao, G. Dai, Y. Hu, L. Lu, L. Chen, P. Cheng, K. Zha, M.A. Shahbazi, Q. Feng, B. Mi, G. Liu, A whole-course-repair system based on neurogenesis-angiogenesis crosstalk and macrophage reprogramming promotes diabetic wound healing, Adv. Mater. 35 (19) (2023) e2212300, https://doi.org/10.1002/adma.202212300.
[60] Y. Hua, K. Wang, Y. Huo, Y. Zhuang, Y. Wang, W. Fang, Y. Sun, G. Zhou, Q. Fu, W. Cui, K. Zhang, Four-dimensional hydrogel dressing adaptable to the urethral microenvironment for scarless urethral reconstruction, Nat. Commun. 14 (1) (2023) 7632, https://doi.org/10.1038/s41467-023-43421-w.
[61] F. Huang, X. Lu, Y. Yang, Y. Yang, Y. Li, L. Kuai, B. Li, H. Dong, J. Shi, Microenvironment-based diabetic foot ulcer nanomedicine, Adv. Sci. 10 (2) (2023) e2203308, https://doi.org/10.1002/advs.202203308.
[62] K. Raziyeva, Y. Kim, Z. Zharkinbekov, K. Kassymbek, S. Jimi, A. Saparov, Immunology of acute and chronic wound healing, Biomolecules 11 (5) (2021), https://doi.org/10.3390/biom11050700.
[63] S. Hu, Z. Yang, Q. Zhai, D. Li, X. Zhu, Q. He, L. Li, R.D. Cannon, H. Wang, H. Tang, P. Ji, T. Chen, An all-in-one "4a hydrogel": through first-aid hemostatic, antibacterial, antioxidant, and angiogenic to promoting infected wound healing, Small 19 (27) (2023) e2207437, https://doi.org/10.1002/smll.202207437.
[64] Y. Wang, Y. Zhang, Y.P. Yang, M.Y. Jin, S. Huang, Z.M. Zhuang, T. Zhang, L.L. Cao, X.Y. Lin, J. Chen, Y.Z. Du, J. Chen, W.Q. Tan, Versatile dopamine-functionalized hyaluronic acid-recombinant human collagen hydrogel promoting diabetic wound healing via inflammation control and vascularization tissue regeneration, Bioact. Mater. 35 (2024) 330–345, https://doi.org/10.1016/j.bioactmat.2024.02.010.
[65] L. Teng, Y. Song, Y. Hu, J. Lu, C.M. Dong, Biomimetic and wound microenvironment-modulating pegylated glycopolypeptide hydrogels for arterial massive hemorrhage and wound prohealing, Biomacromolecules 25 (7) (2024) 4317–4328, https://doi.org/10.1021/acs.biomac.4c00389.
[66] M. Liang, M. Zhang, S. Yu, Q. Wu, K. Ma, Y. Chen, X. Liu, C. Li, F. Wang, Silver-laden black phosphorus nanosheets for an efficient in vivo antimicrobial

application, Small 16 (13) (2020) e1905938, https://doi.org/10.1002/smll.201905938.
[67] Q. Xu, W. Su, C. Huang, H. Zhong, L. Huo, J. Cai, P. Li, Multifunctional polysaccharide self-healing wound dressing: nir-responsive carboxymethyl chitosan/quercetin hydrogel, Adv. Healthcare Mater. (2024) e2403267, https://doi.org/10.1002/adhm.202403267.
[68] L. Huang, J. Deng, Y. Su, X. Hu, Y. Zhang, S. Hong, X. Lin, Thermal-responsive antibacterial hydrogel with photothermal therapy and improving wound microenvironment for promote healing, Antioxidants 13 (7) (2024), https://doi.org/10.3390/antiox13070857.
[69] Y. Wang, C. Chen, C. He, W. Dong, X. Yang, Q. Kong, B. Yan, J. He, Quaternized chitosan-based biomimetic nanozyme hydrogels with ros scavenging, oxygen generating, and antibacterial capabilities for diabetic wound repair, Carbohydr. Polym. 348 (2025) 122865, https://doi.org/10.1016/j.carbpol.2024.122865.
[70] C. Wen, Y. Zhang, L. Lai, X. Zhang, Y. Liu, Q. Guo, R. Peng, Y. Gao, X. Zhang, Y. He, S. Xu, D. Qiao, P. Zheng, Q. Pan, W. Zhu, Photothermally enhanced cascaded nanozyme-functionalized black phosphorus nanosheets for targeted treatment of infected diabetic wounds, Adv. Healthcare Mater. (2023) e2302955, https://doi.org/10.1002/adhm.202302955.
[71] C. Shi, Y. Zhang, G. Wu, Z. Zhu, H. Zheng, X. Sun, Y. Heng, S. Pan, H. Xiu, J. Zhang, Z. Yin, Z. Yu, B. Liang, Hyaluronic acid-based reactive oxygen species-responsive multifunctional injectable hydrogel platform accelerating diabetic wound healing, Adv. Healthcare Mater. 13 (4) (2024) e2302626, https://doi.org/10.1002/adhm.202302626.
[72] X. Zhou, Q. Zhou, Z. He, Y. Xiao, Y. Liu, Z. Huang, Y. Sun, J. Wang, Z. Zhao, X. Liu, B. Zhou, L. Ren, Y. Sun, Z. Chen, X. Zhang, Ros balance autoregulating core-shell ceo(2)@zif-8/au nanoplatform for wound repair, Nano-Micro Lett. 16 (1) (2024) 156, https://doi.org/10.1007/s40820-024-01353-0.
[73] X. Zhang, G. Chen, Y. Liu, L. Sun, L. Sun, Y. Zhao, Black phosphorus-loaded separable microneedles as responsive oxygen delivery carriers for wound healing, ACS Nano 14 (5) (2020) 5901–5908, https://doi.org/10.1021/acsnano.0c01059.
[74] E.L. Mills, B. Kelly, A. Logan, A.S.H. Costa, M. Varma, C.E. Bryant, P. Tourlomousis, J.H.M. Däbritz, E. Gottlieb, I. Latorre, S.C. Corr, G. Mcmanus, D. Ryan, H.T. Jacobs, M. Szibor, R.J. Xavier, T. Braun, C. Frezza, M.P. Murphy, L.A. O Neill, Repurposing mitochondria from atp production to ros generation drives a pro-inflammatory phenotype in macrophages that depends on succinate oxidation by complex ii, Cell 167 (2) (2016) 457–470, https://doi.org/10.1016/j.cell.2016.08.064.
[75] Q. Zhang, W. Gao, Y. Guo, Y. Li, X. Cao, W. Xu, L. Yang, F. Chen, Aqueous enzyme-ultrasonic pretreatment for efficient isolation of essential oil from artemisia argyi and investigation on its chemical composition and biological activity, Ind. Crop. Prod. 158 (2020) 113031, https://doi.org/10.1016/j.indcrop.2020.113031.
[76] L.L. Chen, H.J. Zhang, J. Chao, J.F. Liu, Essential oil of artemisia argyi suppresses inflammatory responses by inhibiting jak/stats activation, J. Ethnopharmacol. 204 (2017) 107–117, https://doi.org/10.1016/j.jep.2017.04.017.
[77] S.S. Scherer, G. Pietramaggiori, J. Matthews, S. Perry, A. Assmann, A. Carothers, M. Demcheva, R.C. Muise-Helmericks, A. Seth, J.N. Vournakis, R.C. Valeri, T. H. Fischer, H.B. Hechtman, D.P. Orgill, Poly-n-acetyl glucosamine nanofibers: a new bioactive material to enhance diabetic wound healing by cell migration and angiogenesis, Ann. Surg. 250 (2) (2009) 322–330, https://doi.org/10.1097/SLA.0b013e3181ae9d45.
[78] M.F. Costa, A.O. Durco, T.K. Rabelo, R. Barreto, A.G. Guimaraes, Effects of carvacrol, thymol and essential oils containing such monoterpenes on wound healing: a systematic review, J. Pharm. Pharmacol. 71 (2) (2019) 141–155, https://doi.org/10.1111/jphp.13054.
[79] H. Wang, S. Sun, Y. Zhao, P. Wang, Y. Zhou, H. Sun, J. Yang, K. Cheng, S. Li, H. Lin, Carbon dots with integrated photothermal antibacterial and heat-enhanced antioxidant properties for diabetic wound healing, Small 20 (45) (2024) e2403160, https://doi.org/10.1002/smll.202403160.
[80] Y. Deng, Y. Gao, T. Li, S. Xiao, M. Adeli, R.D. Rodriguez, W. Geng, Q. Chen, C. Cheng, C. Zhao, Amorphizing metal selenides-based ros biocatalysts at surface nanolayer toward ultrafast inflammatory diabetic wound healing, ACS Nano 17 (3) (2023) 2943–2957, https://doi.org/10.1021/acsnano.2c11448.
[81] M. Rodrigues, N. Kosaric, C.A. Bonham, G.C. Gurtner, Wound healing: a cellular perspective, Physiol. Rev. 99 (1) (2019) 665–706, https://doi.org/10.1152/physrev.00067.2017.
[82] S. Butenko, R.R. Nagalla, C.F. Guerrero-Juarez, F. Palomba, L.M. David, R. Q. Nguyen, D. Gay, A.A. Almet, M.A. Digman, Q. Nie, P.O. Scumpia, M.V. Plikus, W.F. Liu, Hydrogel crosslinking modulates macrophages, fibroblasts, and their communication, during wound healing, Nat. Commun. 15 (1) (2024) 6820, https://doi.org/10.1038/s41467-024-50072-y.
[83] X. Li, R. Bechara, J. Zhao, M.J. Mcgeachy, S.L. Gaffen, Il-17 receptor-based signaling and implications for disease, Nat. Immunol. 20 (12) (2019) 1594–1602, https://doi.org/10.1038/s41590-019-0514-y.
[84] G. Zhao, A. Zhang, X. Chen, G. Xiang, T. Jiang, X. Zhao, Barnacle inspired strategy combined with solvent exchange for enhancing wet adhesion of hydrogels to promote seawater-immersed wound healing, Bioact. Mater. 41 (2024) 46–60, https://doi.org/10.1016/j.bioactmat.2024.07.011.